Transient Response Analysis for Fault Detection and Pipeline Wall Condition Assessment in Field Water Transmission and Distribution Pipelines and Networks

by

Mark Leslie Stephens

February 2008

A Thesis Submitted for the Degree of Doctor of Philosophy

School of Civil and Environmental Engineering
The University of Adelaide, SA 5005
South Australia

Appendix A

Summary of non-hydraulic condition assessment technologies

A.1 Blockage detection technologies

CCTV camera inspection is the most prevalent blockage detection technology (and general condition assessment technology) used in South Australia. United Water commonly uses CCTV cameras to confirm the presence of tuberculation in cast iron and ductile iron distribution pipelines (between 80mm and 300mm in diameter) following steady state flow and pressure testing. The South Australian Water Corporation use CCTV camera inspection when assessing the condition of internal linings and pipe walls at specific locations along larger transmission mains (between 450mm and 1200mm in diameter). Typically, a pipeline is dewatered and cut open to provide access for insertion of a CCTV camera. More recently, pinhole cameras have been inserted through existing access points on “live” pipelines.

A.2 Acoustic leak detection technologies

Acoustic leak detection technologies have become established over the past decade and have been used extensively to reduce leakage in water supply systems in the USA, Europe and Australia. Two variants of the basic methodology, as applied to large and small scale systems, are discussed below.

SAHARA system for large pipelines

The SAHARA leak detection system uses an acoustically sensitive sensor head attached to a long cable to trail along the inside of larger pipelines (greater than 300mm in diameter). The acoustically sensitive sensor listens for leaks as it moves along the inside of the pipeline allowing the location and estimated size of any leak to be directly logged. When a leak is present in a pipe the flow through the leak will generate vibrations through the pipe walls in the ultrasonic range of frequencies

between 5000 and 15000Hz. It is this leak induced noise that the sensor head can detect. Mergelas et al. (2005) have shown that the SAHARA system is capable of detecting leaks as small as 1 litre per hour with accuracy to within 20m.

The sensor head and cable are typically inserted through existing access points along a pipeline and there is no need to either shutdown or dewater the pipeline. The sensor head is carried, by means of a small parachute, in the direction of the flow in the pipeline for up to 2kms. The sensor head includes a tracking emitter that an operator follows above ground as the sensor head trails along inside the pipeline (in the case of a buried pipeline). The only limitations to the SAHARA system are the minimum pipe diameter of 300mm and the problem of secondary faults such as blockages entangling the parachute and probe (Thames Water experience 2004).

Acoustic correlators for pipes less than 300mm in diameter

Instead of a hydrophone being inserted into the pipeline, two accelerometers are attached to the pipeline at a relatively close spacing (typically less than 200m and lower where system topology is complex). These accelerometers are typically installed within existing fire plugs, valves or meter box assemblies. The frequencies in the collected data are compared with the known frequencies emitted by small leaks to determine if one or more leaks are present. After approximately 2 days of data collection at a particular location, the accelerometers are moved to new locations.

Two accelerometers are used to facilitate cross correlation and enable the leak location to be estimated. Providing the accelerometers are located either side of a potential leak, and the leak is not at the midpoint between them, the high frequency noise generated by a single leak travels over a different time and distance to each accelerometers. The cross correlation between the two sets of data will exhibit a maximum correlation at the time lag that corresponds to the delay generated by the additional travel time to the more distant accelerometer. In addition, the relative strength of the signal received at the more distance accelerometer will be reduced. Hunaidi et al. (2000) demonstrated that these effects enable the location of the leak to be accurately determined.

A.3 Wall condition assessment technologies

Conventional condition assessment technologies applicable to pipeline systems, largely developed for the oil and gas industries, include electromagnetic, ultrasonic, magnetic flux leakage, remote field eddy current, seismic pulse echo and CCTV devices (American Water and Wastewater Association, 2004 – Techniques for Monitoring Structural Behaviour of Pipeline Systems). These devices are discussed in further detail below. The application of these technologies to water supply pipelines has been limited because operators have not been able to justify costs against the usefulness of the information obtained. For example, in most cases they give only location specific information (i.e., to the nearest metre or few metres), require internal pipeline access and are not currently easy to insert into pipelines. While the economic case for the use of these technologies in water supply pipelines is developing, and significant research effort is currently devoted to their adaptation to water systems, they remain relatively specialised.

Traditional wall condition assessment

The most common traditional form of assessment is conducted by examining the available historical information for a pipeline. Information regarding pipeline material, time of construction, soil conditions, repair and maintenance history, surcharge loads, external groundwater and the chemical composition of the water (transported in the pipe) is used to develop an understanding of the factors that have contributed to the deterioration of a pipeline over its lifetime.

Other traditional methods of assessment have included exposure of the external surface (if buried) and visual inspection of its condition. Similarly, dewatering of pipelines has been performed to enable internal access, either for a person or CCTV camera, and to allow the extent of internal deterioration of either linings or the pipeline wall to be gauged. Coupon sampling may also be performed and involves the removal of a section or coupon that is then subjected to cleaning and measurement to determine corrosion pit depths (for metallic pipes). In the case of asbestos cement

(AC) pipe, the coupon may be subject to phenolphthalein tests to determine the extent of lime leaching from the cement matrix in the pipe wall.

Broadband electromagnetic probes

Electromagnetic emissions and return signals from an internal probe can be used to directly gauge the thickness of pipe walls made from cast or ductile iron or steel. Probes are typically less than 1m long and need to be in close contact with the internal surface of the pipeline under investigation (around the entire circumference). Provided the probe remains in close contact with the internal pipe face, and is not obstructed by joints or other deposits, it can be used to investigate pipes as small as 80mm in diameter. However, the disadvantages are significant and include the need to depressurise and drain the pipeline, cut the pipe open to provide access for the probe and the slow rate at which the probe can advance (limited to a maximum of 2m per day for larger pipes).

Guided wave ultrasonics

Low frequency ultrasonic waves can be applied externally to steel pipelines with welded joints to assess both internal and external corrosion. The induced waves are sensitive to the distribution and degree of remaining wall thickness. The device needs to be strapped around the circumference of a pipeline and can provide information up to 30m in either direction provided there are no joints or other features changing the thickness of the pipe wall. The pipeline needs to be exposed to enable the device to be attached but otherwise remains operational. The technique can be applied to welded steel pipelines between 50mm and 1200mm in diameter.

Standard ultrasonics

Standard ultrasonic techniques differ from guided wave ultrasonics in that they only provide information at the location of the test (and not up to 30m in either direction). High frequency ultrasonic waves are applied externally to cast iron, ductile iron and steel pipelines and the transmitted waves are attenuated by any discontinuities that may be present. Reflection times between the external and internal faces of the

pipeline can be used to gauge remaining wall thickness. The disadvantages of the technique are that it provides only location specific information per test and that access around the circumference of a buried pipeline is required.

Magnetic flux leakage

A magnetic field is applied externally to cast iron, ductile iron or steel pipelines to assess the total remaining wall thickness. The loss of pipe wall thickness reduces the capacity of the section of pipe under examination to carry the magnetic flux and leakage occurs (which is measured by detectors on the device). The measurements are site specific and the device must be relocated if information at other locations is sought. The disadvantage is that a pipeline needs to be exposed around its entire circumference at each measurement point. The device needs to be calibrated to enable the measured signals to be converted to wall thicknesses.

Remote field eddy current

As for the broadband electromagnetic technique, an electromagnetic field is created inside a cast or ductile iron or steel pipeline. A portion of this field travels along the inside pipe face and is rapidly dissipated by magnetic eddy currents (this portion is called the direct field). The remainder of the field propagates radially through the pipe wall and then travels along the outside pipe face with insignificant dissipation (this portion is called the remote field). At the point of field generation the direct field is stronger than the radially propagated remote field. However, at a distance of approximately 2 to 3 times the pipe diameter along the pipe in either direction, the direct field has dissipated and the remote field, propagating back through the pipe wall, is stronger. A detector coil trails the point of field generation to measure the strength of the remote field which is proportional to the thickness of the pipe wall.

While the device does not need the pipeline to be dewatered to function, the pipeline does need to be depressurised to allow the device to be winched through. Furthermore, the pipeline needs to be internally cleaned (the technique is unsuitable where significant tuberculation has formed). Provided the internal surface of the pipe is clean, the device can be traversed continuously at a rate of approximately 6m per

minute and can be winched through a pipeline for distances of up to approximately 900m.

Seismic pulse echo

Seismic pulse echo (known as "Impact Echo" in Australia) is a sonic technique that can be used to assess delamination and cracking in prestressed concrete pipes and potentially asbestos cement (AC) pipes. The impact from a metal sphere generates shear and sonic waves in the pipe wall. The sonic waves travel more slowly, and with less amplitude, in pipes that have poor wall condition and relative differences are measured by a sensor array. A disadvantage of the technique is that it requires the pipeline to be dewatered to gain internal access. In the case of asbestos cement (AC) pipe, the cutting and access requirements may rule out application of the technique due to occupational health and safety issues.

Soil resistivity tests for metallic pipelines

Relationships between metal pipeline corrosion and soil resistivity can be used as a method for non-destructively gauging external corrosion along an iron or steel pipeline (this is called Linear Polarisation Resistance (LPR) testing in Australia). The technique involves either taking soil samples for laboratory resistivity testing or directly inserting electrodes above the location of a buried metal pipeline and determining the voltage drop between the electrodes to calculate soil resistivity. The spatial density of the sampling and resistivity testing is crucial (typically one sample and test every 50m along a pipeline is the minimum required). Results are sometimes confused if corrosion products from other sources are present in the soil near the pipeline.

Appendix B

Quasi-steady treatment of minor losses under unsteady conditions

Under steady state conditions, the losses associated with minor loss elements such as bends and junctions can dominate where the length of pipe is short relative to the number of minor loss elements. Wood et al. (1993) studied pipe networks dominated by minor loss elements and showed that they were significant when the system had a low slenderness ratio (where the slenderness ratio was defined as the length of pipe divided by its diameter). The same applies under unsteady conditions. That said, the field pipelines and network tested in this research have relatively small numbers of minor loss elements and relatively high slenderness ratios. As a consequence, the influence of minor losses upon the test results was expected to be relatively insignificant. Nevertheless, mechanisms for a quasi-steady determination of unsteady minor losses have been implemented.

B.1 Quasi-steady treatment of in-line orifice or valve

The traditional approach to the treatment of minor losses under transient conditions is to use quasi-steady approximations. This involves adopting the normal flow dependent steady state coefficients for each minor loss element and re-calculating the magnitude of these coefficients, and losses associated with them, as flows vary during a transient event. For example, the presence of a discrete constriction in a pipe may be represented using an in-line orifice at a nodal point in a Method of Characteristics (MOC) grid. The pressure loss can be solved explicitly at a point in time using the two compatibility equations for the adjacent pipe computational units and the steady state in-line orifice equation at the node:

$$Q_{orf} = C_d A_{orf} \sqrt{2g\Delta H_{orf}} \qquad \text{(B-1)}$$

where Q_{orf} is the flow through the in-line orifice, C_d is the coefficient of discharge, A_{orf} is the area of the in-line orifice and ΔH_{orf} is the pressure loss across the in-line orifice

The steady state in-line orifice and valve equations are identical, if the area of the orifice and valve are substituted, and either can be used to approximate the response of a discrete constriction during a transient event. However, the steady state in-line valve equation is traditionally presented, in terms of a dimensionless valve position, as:

$$Q_V = \tau \, C_V \sqrt{\Delta H_V} \tag{B-2}$$

where Q_V is the flow through the in-line valve, $\tau = \frac{C_d A_V}{(C_d A_V)_0}$ and $C_V = \frac{Q_0}{\sqrt{(\Delta H_V)_0}}$

B.2 Quasi-steady treatment of other minor loss elements

Unfortunately, there are no analytical solutions, except for an abrupt expansion, with which to determine the magnitude of loss associated with other minor loss elements under particular flow conditions (whether steady or unsteady). This is because of physically complex eddy formation and flow separation that occurs at such elements. These effects have been experimentally observed by many researchers, under steady state conditions, and require the empirical calibration of loss coefficients (*K* factors) for each minor loss element. Idel'Chik (1960) and Miller (1976) have conducted exhaustive experiments establishing steady state loss coefficients for various geometries and flow configurations for typical bends and junctions.

The steady pressure loss associated with a bend can be calculated using:

$$\Delta H = K_b \frac{V^2}{2g} \tag{B-3}$$

where K_b is a loss coefficient that varies between values of 0.2 and 1.5 with the angle of deflection of the bend, the ratio of the radius of curvature of the bend to pipe diameter and the Reynolds number of the flow

Similarly, the steady pressure loss associated with a typical T-junction can be calculated using:

$$\Delta H_{t1} = K_{t1}\frac{V_{t1}^2}{2g},\ \Delta H_{t2} = K_{t2}\frac{V_{t2}^2}{2g} \text{ and } \Delta H_{t3} = K_{t3}\frac{V_{t3}^2}{2g} \tag{B-4}$$

where K_{t1}, K_{t2} and K_{t3} are the loss coefficient applicable to each leg of the junction, as shown in Figure B-1, for different flow configurations

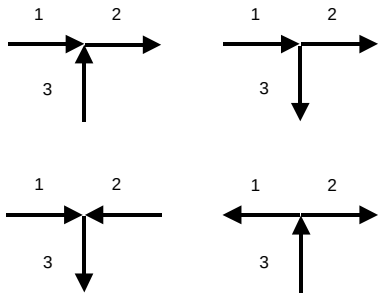

Figure B-1 – Steady flow configurations for a T-junction

The effect of a bend or junction can be incorporated in a forward transient model by including an equivalent pipe length, with a zero time lag with respect to the transmission of the transient wavefront, to replicate the pressure loss associated with the minor loss element. The equivalent pipe length is set such that the friction loss along it matches the loss estimated using the steady pressure loss coefficients and flows discussed above. In the case of a typical T-junction, equivalent pipe lengths can be inserted on each of the three arms of the junction. The steady state loss coefficients for each minor loss element are re-calculated during the transient event using the flows from the previous time step and equivalent lengths are re-determined. The flow through these elements can then be solved explicitly, at the current time step, using

the compatibility equations from the adjacent pipe computational units and the steady state relation describing the pressure loss across the minor loss element:

$$\Delta H = K_e \frac{Q^2}{2gA^2} \tag{B-5}$$

where K_e is the loss coefficient for the relevant minor loss element and Q and A are the flow within and area of the equivalent pipe

The distinction between the calculation of the magnitude of the minor loss associated with a bend and a T-junction is that the flow through the bend is limited to two states (either positive or negative) whereas the flow through the T-junction has four possible configurations. This requires an iterative re-determination of the flow in each of the arms of the T-junction at each time step throughout a transient calculation. The magnitude of the applicable loss coefficient in each arm on the T-junction depends on the flow in the arm and the overall flow configuration. The loss coefficients for the different flow configurations can be calculated using the relationships presented by Miller (1976).

The above methodology for incorporating minor losses during a transient has been implemented in the explicit and implicit MOC pipeline and network models developed in this research. It is possible that the loss coefficients associated with bends and T-junctions under unsteady flow conditions vary from those applicable at any equivalent steady state condition because of unsteady inertial and shear effects. While Idel'Chik (1960) and Miller (1976) have experimentally determined minor loss coefficients for a range of geometries and flows under steady conditions, no such coefficients have been experimentally determined under unsteady conditions apart from investigations into in-line orifices and valves, as described in the thesis, and recent work, relating to T-junctions, conducted by Prenner (2000).

Appendix C

Derivation of least squares criteria from maximum likelihood theory

Maximum likelihood theory forms the foundation of inferential regression analysis. If h^* is a vector incorporating all of the observed pressure data for a particular transient response, and B is a vector of unknown model parameters that contribute to the prediction of the corresponding transient response, then the likelihood $L(B/h^*)$ of a hypothesis regarding the parameter values in vector B, given the observed pressure data h^*, and a particular model structure, is proportional to the probability $f(h^*,B)$ of observing h^* if B was true. Since $L(B/h^*)$ is dependent on the parameter values in vector B it is referred to as a likelihood function.

The normal distribution is the most widely assumed probability model. The probability density function of the normal distribution for a single random variable x is:

$$f\left(x/\mu,\sigma^2\right)=\frac{1}{\sigma\sqrt{2\pi}}\exp\left[-\frac{1}{2}\left(\frac{x-\mu}{\sigma}\right)^2\right] \qquad \text{(C-1)}$$

where μ and σ^2 are the mean and variance of the random variable x

The mean and variance of the random variable x have expected or "true" values for which the probability density function expressed in Equation C-1 is valid. In the case of Inverse Transient Analysis (ITA), we have an observed pressure data vector h^* (for random variable x) and an expected or "true" pressure response vector h (instead of the expected mean value μ). A covariance matrix Σ for the observed pressure data vector h^* is introduced instead of σ^2. It is assumed that vector h has expected or "true" values for which the normal probability density function is valid. It will be demonstrated below that this assumption implies the least squares minimisation criterion is applicable.

Appendix C – Derivation of least squares criteria from maximum likelihood theory

The expected or "true" pressure response vector *h* will be obtained, assuming the model structure is correct, if the values in the parameter vector *B* are also "true" (i.e., because the values obtained for *h* are a function of *B*). Hence, the probability of obtaining the observed pressure data vector h^*, if the values in the parameter vector *B*, and hence the expected pressure response vector *h*, are "true", is the relevant reformulation of the problem:

$$L\left(B/h^*\right) \propto f\left(h^*/h,\Sigma\right) = \frac{1}{(2\pi)^k}|\Sigma|^{-1}\exp\left[-\frac{1}{2}\left(h^*-h\right)^T\Sigma^{-1}\left(h^*-h\right)\right] \qquad \text{(C-2)}$$

where h^* is a vector incorporating all of the observed pressure data and *h* is the "true" pressure response as determined for the "true" parameter values in vector *B*

However, the "true" pressure response is not known (i.e., the "true" parameter values in vector *B* are not known). In fact, the purpose of the regression analysis is to determine the most appropriate values for vector *B*. It is necessary to substitute the "true" with predicted pressure response in Equation C-2 to obtain:

$$L\left(\hat{B}/h^*\right) = f\left(h^*/\hat{B}\right) \propto \frac{1}{(2\pi)^k}|\Sigma|^{-1}\exp\left[-\frac{1}{2}\left(h^*-\hat{h}\right)^T\Sigma^{-1}\left(h^*-\hat{h}\right)\right] \qquad \text{(C-3)}$$

where $\hat{h}$ is the predicted pressure response (a function of the predicted values in the parameter vector $\hat{B}$)

The multiplication of the transposed $\left(h^*-\hat{h}\right)^T$ and non-transposed $\left(h^*-\hat{h}\right)$ vectors in the exponential term of Equation C-3 can be performed for a fixed covariance matrix Σ. This gives rise to a summation of the squares of the differences between the observed pressure data and the predicted pressure response (determined for a particular model). If the summation of the squares of the differences is minimised, then the likelihood function is maximised (i.e., if the parameter values in the vector $\hat{B}$ give rise to a predicted pressure response $\hat{h}$ that minimises the sum of the square of

the differences with the observed pressure data h^* then the likelihood of $\hat{B}$ is maximised). This represents a restatement of the classic least squares minimisation criterion:

$$L\left(\hat{B}/h^*\right) \propto \min \sum_{t=1}^{n} \left[h_t^* - \hat{h}_t\left(\hat{B}\right)\right]^2 \qquad \text{(C-4)}$$

where n is the total number of data points in the observation vector h_t^* and $\hat{h}_t\left(\hat{B}\right)$ is a function of the parameter values in the vector $\hat{B}$

Appendix D

Geometric details and laboratory tests on Asbestos Cement (AC) pipe

D.1 The prevalence of AC pipes

Asbestos Cement (AC) pipe is a common class of pipe in networks in many countries throughout the world. In the United Kingdom, it is estimated that there is approximately 200,000 km of AC pipes comprising approximately 20% of the water distribution systems in the country (Thames Water 2004). In the City of Adelaide, South Australia, approximately 50% of the water distribution system is comprised of AC pipe. Hu and Hubble (2005) recently examined AC pipe failure rates in the City of Regina, Canada, where approximately two thirds of the water distribution system comprised AC pipelines. The Willunga Network, tested in this research, exclusively comprises AC pipe.

D.2 Geometric details and construction dates for pipes comprising the Willunga Network

The Willunga Network comprises 100mm to 150mm nominal diameter Asbestos Cement (AC) pipe with a short length of 250mm nominal diameter AC pipe. The geometric details for 100mm, 150mm and 250mm nominal diameter AC pipe are listed in Table D-1 below (and are based on details from obsolete Australian Standard AS 1711 – 1975).

Table D-1 – Geometric properties for AC pipes comprising the Willunga Network

Nominal Diameter (mm)	Class	Min. wall thickness (mm)	External diameter (mm)	Internal diameter (mm)
100	D	12.7	121.9	96.5
150	D	17.8	177.3	141.7
250	D	27.5	286.0	231.0

The Willunga Network was constructed, in a piecemeal fashion, over an extended period of time. Different sections were constructed somewhere in the period from 1963 to 1986. Table D-2 lists the specific years in which particular AC pipes (along streets identified in Chapter 15 of the thesis) were constructed within the Willunga Network:

Table D-2 – Construction year for sections of AC pipe within the Willunga Network

Street or section	Year	Size (mm)
St Marys Street – section on south side of Victor Harbour Freeway and connected to Willunga tank	1975	250
St Marys Street – section to Church Street intersection	1963	250
Church Street section to Willunga pump station	1963	250
St Marys Street – section between Church Street and St Judes Street	1986	150
St Judes Street	1963	100
Bishop Street	1963	100
St Georges Street	1976	100
High Street from intersection with St Judes Street westward	1963	150
High Street from intersection with St Judes Street to dead end	1963	100
Moore Street	1963	100
Bridge Street	1974	100
St Lukes Street	1963	100
St James Street	1963	100

D.3 Laboratory tests for elastic properties of AC pipe

Taunton (1983) examined the material properties of Asbestos Cement (AC) pipe and confirmed that they comprise approximately 86% Portland Cement and 14% asbestos fibres and have typical bursting and crushing stresses of 30 and 60MPa, respectively. Stokes (1983) confirmed bursting and crushing stress values of 30 to 32MPa and 60 to 65MPa, respectively. The asbestos fibres were found to chemically bond with the cement during the hydration process. The resulting AC was homogeneous and isotropic with fibres orientated to provide mechanical strength in both axial and circumferential planes.

Appendix D – Geometric details and laboratory tests on Asbestos Cement (AC) pipe

Unfortunately, the last Australian Standard applicable to the use of AC pipe in water distribution systems (Australian Standard 1711 – 1975: "Asbestos Cement Pressure Pipes") was withdrawn in July 1990 and contained little information on the material properties of AC pipe. A sample of AC pipe from the WN was therefore subjected to stress/strain tests to determine its elastic properties. The sample comprised a section of "class D" AC pipe approximately 800 mm long with an internal diameter of 96.5mm and wall thickness of 12.7mm. Four 68mm Demac strain gauges were attached to the sample (orientated in the axial direction).

The testing was difficult to organise and conduct because of the stringent safety standards that apply to the handling of asbestos products and only non-destructive testing of the sample was permitted. Given these constraints, it was decided to perform axial compression tests on the sample to determine whether it deformed elastically under linearly increasing load. Because the AC pipe material is both homogenous and isotropic, Poisson's ratio could be used to estimate the strain in the circumferential plane even though the sample was loaded in axial compression. The Poisson's ratio for concrete is approximately 0.2 and this value has been adopted in the calculations. The tests performed are summarised in Table D-3:

Table D-3 – Measured loads and strains for compression tests on AC pipe sample

Test	Maximum Load (kN)	Time to load up to maximum (s)	Maximum Axial Stress (MPa)	Maximum Axial Strain	Maximum Circumferential Strain
1	80.8	180	18.5	589×10^{-6}	118×10^{-6}
2	81.3	20	18.7	585×10^{-6}	117×10^{-6}
3	81.2	20	18.6	590×10^{-6}	118×10^{-6}
4	80.9	20	18.6	587×10^{-6}	117×10^{-6}
5	81.3	20	18.7	589×10^{-6}	118×10^{-6}

Figures D-1 and D-2 show the strain versus load response of the AC pipe sample when subject to slow (180s) and fast (20s) loading rates, respectively. It was important to conduct a set of tests with fast loading rates (tests 2, 3, 4 and 5) in order

to check for non-linear behaviour over time scales similar to those of the transients in the Willunga Network.

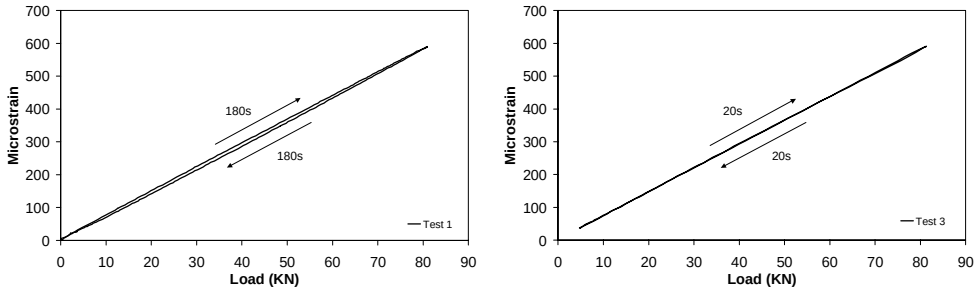

Figures D-1 and D-2 – Load versus strain relationship for AC pipe sample under axial compression for 180s (slow) and 20s (fast) loading rates

For the test load range, the AC pipe sample displayed linear elastic behaviour, under axial compression, independent of the rate of loading. The average value for the modulus of elasticity was approximately 32GPa. This value is typical of that for high strength concrete and is greater than that specified in the Australian Design Manual produced by Hardie Industries (which specifies a minimum modulus of elasticity of 21.4GPa for AC pipe). The effect of an increase in the modulus of elasticity of the asbestos cement from 21GPa to 32GPa, upon wave speed, is illustrated in Table D-4 assuming a Poisson's ratio of 0.2 and the pipeline is restrained from axial movement.

Table D-4 – Sensitivity of wave speed for AC pipe to change in elastic modulus

Nominal Diameter (mm)	Wave speed for E=21GPa (m/s)	Wave speed for E=32Gpa (m/s)
100	1108	1200
150	1097	1191
250	1084	1180

The maximum axial stress for test 1of 18.5MPa (when the sample was under a load of 80.8kN) gives an inferred circumferential stress of 3.7MPa. This level of circumferential stress is equivalent to the circumferential stress that would develop in a section of AC pipe under a hydrostatic pressure of 974kPa (which exceeds the

maximum hydrostatic pressure in the Willunga Network of 800kPa). The results form a basis upon which to conclude that AC pipe is inherently elastic. However, without results from specialised apparatus, capable of applying rapid load changes over time scales in the order of milliseconds, the possibility of non-elastic or viscoelastic behaviour cannot be completely discounted. In this regard, reference is made to the statements by researchers who have performed tests using specialised apparatus and indicated that cement pipes are not viscoelastic. Covas (2002b) confirmed that cement behaves in a linear elastic fashion and that viscoelastic modelling is not required to simulate the response of a cement pipe to a transient event.

In addition to the stress/strain tests described above, a creep test was performed to assess the behaviour of the AC pipe material under a sustained load of 40kN for 3 hours. The AC pipe sample exhibited no creep deformation over the test period.

Appendix E

Unsteady friction algorithms and recursive approximations

E.1 Conceptualisation of unsteady friction

Unsteady friction arises in transient flow situations when rapid changes result in the dissipation of shear energy at the wall of a pipe. Lambert et al. (2001) provided a physical explanation for the process of energy dissipation in terms of the cyclic growth and destruction of boundary layers in the flow. In the case of a pipeline with an established steady flow, the boundary layer within the pipeline will be fully developed and extend to the centre of the pipe. If an in-line valve is suddenly closed, and the flow velocity is reduced to zero as the transient wavefront propagates along the pipeline, the existing boundary layer will dissipate. Little additional friction loss is associated with this decelerating flow as confirmed by Daily et al. (1956).

However, if the transient is cyclic, and the wavefront can reflect off a boundary such as a tank, a reverse flow will begin to establish itself as the transient continues to propagate. As this reverse flow becomes established (i.e., accelerating flow in the reverse direction to the initial steady flow), a new boundary layer begins to form and continues to develop, propagating radially towards the centre of the pipe, until another flow reversal from a subsequent reflection of the transient wave occurs. Greater friction loss, than that predicted on a quasi-steady basis, occurs because of the high shear stresses that develop during the initial growth of the new boundary layer.

The above conceptualisation does not account for the concentration of the friction effects in the boundary layer close to the pipe wall or the possibility of the wall shear stress moving in and out of phase with the mean velocity of the transient flow. The propagation of the transient event will first affect the boundary layer and shear stress, which remains in phase with the transient wavefront, at the pipe wall. However, the bulk of the flow away will continue to be dominated by its inertia and will remain in phase with the acceleration of the fluid. This effect may mean that the flow in the boundary layer will be moving in one direction while the bulk of the flow and mean

velocity is in the other direction. It is apparent that this effect is two-dimensional and that the diameter of a pipeline will directly influence the relative interaction of the boundary layer and bulk flow away from the pipe wall.

E.2 Weighting function method for laminar flow

Formulation developed by Zielke (1968)

One-dimensional weighting function models for unsteady friction involve the convolution of a weighting function with the flow history throughout a transient event to calculate the contribution of unsteady friction to total friction loss. Zielke (1968) first derived an analytical expression, for laminar flow conditions only, relating wall shear stress to the instantaneous velocity and weighted past velocity changes:

$$\tau_0(t) = \frac{4\rho\nu}{R}V(t) + \frac{2\rho\nu}{R}\int_0^t \frac{\partial V}{\partial t}(u)W(t-u)du \qquad \text{(E-1)}$$

where τ_0 is the total wall shear stress, ρ is the fluid density, ν is the kinematic viscosity, R is the pipe radius, V is the mean velocity, u is the time used in the convolution integral and W is the weighting function derived by Zielke (1968) as expressed below:

$$W(\tau) = 0.282\tau^{-1/2} - 1.250 + 1.058\tau^{1/2} + 0.938\tau + 0.397\tau^{3/2} - 0.352\tau^2 \qquad \text{(E-2)}$$

with dimensionless time $\tau = \frac{\nu}{R^2}t > 0.02$

Zielke (1968) incorporated the solution for unsteady wall shear stress losses into the Method of Characteristics (MOC) solution for transient flow and pressure by modifying the determination of the friction component to include both a quasi-steady and unsteady effect:

$$h_f = h_{fS} + h_{fU} \qquad \text{(E-3)}$$

The unsteady component, $h_{fU,}$ was calculated by convolving the velocity changes throughout the transient with an unsteady friction weighting function W for laminar flow:

$$h_f = \frac{32\nu}{gD^2}V(t) + \frac{16\nu}{gD^2}\int_0^t \frac{\partial V}{\partial t}(u)W(t-u)du \tag{E-4}$$

which can be re-expressed, in terms of flow and pipe area, as:

$$h_f = \frac{fQ|Q|}{2gDA^2} + \frac{16\nu}{gD^2A}\left(\frac{\partial Q}{\partial t} * W\right)(t) \tag{E-5}$$

where the second term represents the calculation of the unsteady friction component

The term in the brackets represents the convolution of the change in flow with the unsteady friction weighting function for laminar flow. Changes in flow are multiplied with the weighting function, and integrated over the time history of the entire transient event, to perform the convolution using:

$$\left(\frac{\partial Q}{\partial t} * W\right) = \int_0^t \frac{\partial Q}{\partial t}(t')W(t-t')dt' \tag{E-6}$$

Zielke (1968) demonstrated that this integral could be numerically evaluated at a particular point in time (i) and space (k) in a MOC grid using:

$$\left(\frac{\partial Q}{\partial t} * W\right)_{i,k} = (V_{i,k} - V_{i,k-1})W(\Delta t) + (V_{i,k-1} - V_{i,k-3})W(3\Delta t) + \ldots + (V_{i,3} - V_{i,1})W((k-1)\Delta t) \tag{E-7}$$

The above implementation of a one-dimensional weighting function model provides for the accurate calculation of unsteady friction, for laminar flow conditions, in

pipelines and networks subject to transients. It has been implemented in the single pipeline and network transient models developed in this research. However, the convolution of the weighting function and flow history over the duration of the transient event is extremely computationally intensive.

Efficient recursive approximations for unsteady friction in laminar flow

While not as computationally taxing as two-dimensional models, the one-dimensional weighting function model developed by Zielke (1968) is nevertheless inefficient because it needs to store and continuously recall flows (or velocities) from the beginning of the transient to perform the convolution with the weighting function and calculate the unsteady component of the total friction (h_{fU}) at each time step. The calculation of h_{fU} may be performed more efficiently using the recursive approximations developed by Trikha (1975) and refined by Kagawa et al. (1983).

Trikha (1975) defined Zielke's weighting function in terms of an approximate weighting function:

$$W_{app}(\tau) = m_1 e^{-n_1\tau} + m_2 e^{-n_2\tau} + m_3 e^{-n_3\tau} \tag{E-8}$$

where W_{app} is an approximate weighting function, τ is dimensionless time and n_k and m_k are coefficients for k equal to 1, 2 and 3, respectively

The values of the coefficients n_k and m_k were determined by fitting Zielke's weighting function and the approximate function at dimensionless times 0.0001, 0.001 and 0.01. The unsteady component of the total friction could then be calculated using:

$$h_{fU}(t) = \frac{16\nu}{gD^2}\left[y_1(t) + y_2(t) + y_3(t)\right] \tag{E-9}$$

with the recursive variables y_k defined as:

$$y_k(t+\Delta t) \approx e^{-n_k K\Delta t} y_k(t) + m_k\left[V(t+\Delta t) - V(t)\right] \tag{E-10}$$

where K is a constant used to convert dimensionless time and is equal to $4\nu/D^2$

Instead of needing to store and continuously recall the flow history to perform convolutions, Trikha (1975) only required the storage of three recursive variables and the flow at the previous time step. However, the use of only three exponents to represent the approximate weighting function compromised the solution accuracy. Kagawa et al. (1983) improved the accuracy of the approximation, without any significant loss in computational efficiency, by fitting ten exponential terms.

The approach used by Kagawa et al. (1983) is elaborated below in some detail because it forms the basis upon which the unsteady friction calculations have been performed in the research described in this thesis. It also forms the basis of the efficient approximation of unsteady friction for smooth/rough pipe turbulent flow. Furthermore, the principle of using a recursive approximation to improve computational efficiency has also been applied in the development of an efficient algorithm for the calculation of viscous and viscoelastic damping as described in Chapter 5.

Kagawa et al. (1983) defined an approximate weighting function for the calculation of unsteady friction in laminar flow as:

$$W_{app}(\tau) = \sum_{k=1}^{N} m_k e^{-n_k \tau} \tag{E-11}$$

Values for the exponential parameters m_k and n_k are determined by fitting to the true weighting function (only needs to be done once using an optimisation algorithm). The value of k varies with the value of $\Delta\tau$ (the dimensionless time step equal to $4\nu\Delta t/D^2$). Kagawa et al. (1983) determined a value for k of 10. The unsteady component of the total friction could then be calculated using:

$$h_{fU}(t) = \frac{16\nu}{gD^2} \sum_{k=1}^{N} y_k(t) \tag{E-12}$$

in which the recursive variables y_k are defined as:

$$y_k(t) = \int_0^t \frac{\partial V}{\partial t'} m_k e^{-n_k K(t-t')} dt' \tag{E-13}$$

where t' is the convolution time and K is $4\nu/D^2$

and

$$y_k(t+\Delta t) = \int_0^{t+\Delta t} \frac{\partial V}{\partial t'} m_k e^{-n_k K(t+\Delta t-t')} dt' \tag{E-14}$$

Splitting the integral range into (0, t) and (t, $t+\Delta t$), and substitution for the integral over the later range, gives an expression for the recursive variables at the current time step in terms of those stored for the previous time step, the flows at the current and previous time steps and the dimensionless time step ($\Delta\tau$ equal to $K\Delta$t):

$$y_k(t+\Delta t) = e^{-n_k \Delta\tau}\left(e^{-n_k \Delta\tau} y_k(t) + m_k\left[V(t+\Delta t) - V(t)\right]\right) \tag{E-15}$$

The values of ten recursive variables (y_k) need to be stored, at each spatial point in any MOC model, and updated on an on-going basis. However, as demonstrated by Vitkovsky et al. (2004), the Kagawa et al. (1983) approximation does not significantly compromise the solution accuracy.

E.3 Weighting function method for smooth/rough pipe turbulent flow

Full convolution of 1-D weighting function

While Zielke (1968) has developed a one-dimensional weighting function model for the calculation of unsteady friction for laminar flow, the analytical solution applied cannot be readily transferred to turbulent flow situations because of the presence of eddy viscosity. The Laplace transform used by Zielke (1968) cannot be applied to the

resulting system of non-linear equations. Vardy and Brown (1995) overcame this obstacle, to determine a one-dimensional weighting function for smooth pipe turbulent flow, by assuming that the viscosity for smooth pipes under turbulent flow conditions varied linearly within a relatively thick shear layer surrounding a core of uniform viscosity. Laplace transforms were taken of the equations of motion for the shear layer and core of uniform viscosity by assuming this spatial distribution remained "frozen" throughout the duration of the transient.

The expressions for the transformed shear stress in the shear layer and core of uniform viscosity were equated at the interface between the two zones. The resulting velocity distributions enabled the determination of an analytic expression for the Laplace transform representing the total friction for the unsteady flow case. The process was repeated for the steady flow case and the unsteady component extracted, by subtracting the Laplace transform obtained for the unsteady flow from that for the steady flow, to obtain the transformed wall shear stress due to unsteady friction.

As for the method elaborated by Zielke (1968), Vardy and Brown (1995) were then able to equate the unsteady component of the wall shear stress to the transformed acceleration and a weighting function. Zielke (1968) used the following relation:

$$\tau_{wU}^{'} = \frac{2\rho\nu W^{'}}{R}\left(\frac{\partial V}{\partial t}\right)^{'} \tag{E-16}$$

where the subscripts *w* and *U* stand for wall and unsteady, ρ is the fluid density, ν is the kinematic viscosity, *W* is the weighting function, *R* is the pipe radius and *V* is the mean velocity

The relation used by Vardy and Brown (1995) is not elaborated here but is essentially similar. The weighting function for smooth pipe turbulent flow was then obtained by approximating the transformed weighting function with a simpler function:

$$W_a^{'}(s) = \frac{A}{\sqrt{s+B}} \tag{E-17}$$

where the subscript *a* denotes approximation, *s* is the Laplace transform variable and *A* and *B* are constants for particular values of Reynolds number and pipe roughness

The inverse of this approximated and transformed weighting function was then taken to get the untransformed weighting function. While the full derivation presented by Vardy and Brown (1995) is not reproduced here, the final expression for the weighting function is:

$$W_a(t) = \frac{A\exp(-Bt)}{\sqrt{\pi t}} \tag{E-18}$$

where the subscript *a* denotes the approximation made prior to inverse transformation and:

$$A = \frac{R}{2\sqrt{\nu}} \text{ and } B = 0.135(\nu/R^2)\mathrm{Re}^{\kappa} \tag{E-19}$$

where R is the pipe radius, ν is the kinematic viscosity, Re is the Reynolds number and $\kappa = \log_{10}(14.3/\mathrm{Re}^{0.05})$

The above weighting function can be effectively substituted for that used in Zielke's formulation for laminar flow in the MOC. The parameters *A* and *B* are calculated on the basis of the values for the viscosity and Reynolds number under steady conditions.

While the above formulation catered for smooth pipe turbulent flow, methods for the calculation of unsteady friction for rough pipes under turbulent flow conditions remained undetermined. Silva-Araya and Chaudry (2001) presented a method incorporating an eddy viscosity model in an outer shear layer to calculate the wall shear stresses for flow in rough walled pipes. An inner core of flow was assumed and a mixing-length distribution model used to blend the transition from the outer to inner layer.

Vardy and Brown (2004a) developed a one-dimensional weighting function model for the calculation of unsteady friction for rough pipes under turbulent flow conditions in a similar fashion to the smooth pipe turbulent flow case by using a two-dimensional unsteady friction model for calibration. The main difference lay in the form of the transformed weighting function for rough pipes under turbulent flow conditions with the result that dimensionless constants A^* and B^* are calculated using:

$$A^* = 0.0103\sqrt{\mathrm{Re}}\left(\frac{\varepsilon}{D}\right)^{0.39} \quad \text{and} \quad B^* = 0.352\,\mathrm{Re}\left(\frac{\varepsilon}{D}\right)^{0.41} \tag{E-20}$$

where Re is the Reynolds number, ε is the roughness height of the inside of the pipe wall and D is the pipe diameter

However, Vardy and Brown (2004a) still relied on the storage of all flow and head values in both time and space when convolving the smooth/rough pipe turbulent flow weighting functions with the stored flow history throughout a transient event. This meant that the procedure for using one-dimensional weighting functions to calculate unsteady friction, while now adapted for smooth/rough pipe turbulent flow, remained computationally demanding.

Efficient approximation of unsteady friction for smooth/rough pipes

Ghidaoui and Mansour (2002) developed a recursive approximation for the smooth pipe turbulent flow weighting function model developed by Vardy and Brown (1995). While improving efficiency, the proposed recursive approximation comprised solution accuracy. Vardy and Brown (2004b) proposed an efficient approximation that did not require the use of a recursive approximation. As for the case of laminar flow, the objective was to determine an approximation to the equation:

$$h_{fU}(t+\Delta t) = \frac{16\nu}{gD^2}\int_0^{t+\Delta t}\frac{\partial V}{\partial t}(u)W_a(t+\Delta t-u)\,du \tag{E-21}$$

in which W_a is the approximate weighting function for smooth pipe turbulent flow

Following the methods developed by Trikha (1975) and Kagawa et al. (1983), Vardy and Brown (2004b) split the integral range into (0, t) and (t, $t+\Delta t$). However, instead of substituting for the integral over the later range to set up a recursive approximation, Vardy and Brown (2004b) determined separate exponential approximations for each partial integral:

$$I_1 \equiv \int_0^t \frac{\partial V}{\partial t}(u) W_a(t+\Delta t-u)du \approx Y_a(t)e^{C\Delta t} \tag{E-22}$$

where Y_a is the stored approximate value for the unsteady friction up to time t and C is a constant

and

$$I_2 \equiv \int_t^{t+\Delta t} \frac{\partial V}{\partial t}(u) W_a(t+\Delta t-u)du \approx \frac{DU}{G}\left(1-e^{-G\Delta t}\right) \tag{E-23}$$

where D is the pipe diameter, U is the average acceleration of the mean flow over the time interval (t, $t+\Delta t$) and G is a coefficient equal to the negative of C

The result was an expression for the unsteady component of the total friction in terms of:

$$h_{fU}(t+\Delta t) = \frac{16\nu}{gD^2}\left[Y_a(t)e^{-G\Delta t} + \frac{DU}{G}\left(1-e^{-G\Delta t}\right)\right] \tag{E-24}$$

Alternatively, Vitkovsky et al. (2004) directly adapted the efficient recursive approximations developed for laminar flow by Trikha (1975) and Kagawa et al. (1983) to smooth and rough pipe turbulent flow conditions. As elaborated above, the weighting function for these conditions takes the form:

$$W(\tau) = \frac{A^* e^{-B^* \tau}}{\sqrt{\tau}} \tag{E-25}$$

in which:

$A^* = \frac{1}{2\sqrt{\pi}}$ and $B^* = 0.135\,\mathrm{Re}^{\kappa}$ are dimensionless coefficients for smooth pipe flow

with $\kappa = \log_{10}(14.3\,\mathrm{Re}^{-0.05})$ (E-26)

and

$A^* = 0.0103\sqrt{\mathrm{Re}}\left(\frac{\varepsilon}{D}\right)^{0.39}$ and $B^* = 0.352\,\mathrm{Re}\left(\frac{\varepsilon}{D}\right)^{0.41}$ for rough pipe flow (E-27)

Vitkovsky et al. (2004) followed a similar procedure to that adopted by Kagawa et al. (1983) in order to fit an approximate weighting function. However, in the case of turbulent flow, the magnitude of the coefficients A^* and B^* are dependent upon the Reynolds number of the flow (and hence the initial conditions) and, for rough pipes, the relative roughness of the pipe(s). Vitkovsky et al. (2004) overcame this problem by scaling the fitted values of the exponential parameters m_k and n_k using values of A^* and B^* determined for each pipe's initial flow condition and/or roughness:

$$W^*_{app}(\tau) = \sum_{k=1}^{N} m^*_k e^{-n^*_k \tau} \tag{E-28}$$

in which:

$m^*_k = m_k / A^*$ and $n^*_k = n_k - B^*$ are the scaled exponential parameters (E-29)

Values of m_k and n_k, determined for laminar and turbulent flow conditions, can be obtained from Vitkovsky et al. (2004) and have been used, with the recursive approximations for laminar flow, developed by Kagawa et al. (1983), and for smooth/rough pipe turbulent flow, as described above, for the calculation of unsteady

friction throughout this research. The author independently implemented software that was used to verify the efficient recursive algorithm developed by Vitkovsky et al. (2004) and was the second author for that publication.

E.4 Instantaneous flow acceleration based models

One-dimensional flow acceleration models for unsteady friction have been postulated since the mid-1950s with the more recent models proposed by Brunone et al. (1991) and Vitkovsky et al. (2005). In essence, an additional unsteady friction loss is determined based on the instantaneous acceleration of the flow using numerically or experimentally calibrated formulations. The typical formulation is:

$$h_{fU} = \frac{k}{g}\left(\frac{\partial V}{\partial t} - a\frac{\partial V}{\partial x}\right) \tag{E-30}$$

where h_{fU} is the unsteady component of the total friction loss and coefficient k is numerically determined from a more physically accurate model or experimentally calibrated

Vitkovsky et al. (2005) modified this typical formulation to reflect the distinction between the temporal and convective acceleration components and allow the separate calibration of k_P and k_A coefficients:

$$h_{fU} = \frac{k_P}{g}\frac{\partial V}{\partial t} + \frac{ak_A}{g}\frac{\partial V}{\partial x} \tag{E-31}$$

where the coefficient k_P is analogous to a momentum correction factor (and provides for a phase related wave speed change) and the k_A coefficient incorporates extra friction damping due to unsteady shear stresses and is magnitude related

Vitkovsky et al. (2005) explain that the application of instantaneous flow acceleration based models is complicated by the reality that there are eight possible flow and wavefront direction and acceleration combinations that can exist during a transient. In the case of positive flow along a pipeline, the transient wave can be propagating

upstream or downstream and be either accelerating or decelerating. Hence, four potential flow, wavefront direction and acceleration combinations are possible for positive flow along a pipeline. Similarly, four potential flow, wavefront direction and acceleration combinations are possible for negative flow along a pipeline (where positive and negative flow are arbitrarily defined).

Vitkovsky et al. (2005) introduced a phase coefficient (ϕ_A) to account for the direction of the convective acceleration during a transient and derive a modified version of Equation E-31:

$$h_{fU} = \frac{k_P}{g}\frac{\partial V}{\partial t} + \frac{a\phi_A k_A}{g}\frac{\partial V}{\partial x} \tag{E-32}$$

While the model was able to accurately replicate measurements for valve closures and improved the model presented by Brunone et al. (1991), Vitkovsky et al. (2005) found that the model was incapable of replicating the transient response from an in-line valve opening. Furthermore, instantaneous flow acceleration based models do not replicate the frequency dependant nature of unsteady friction. This leads to numerical attenuation and dispersion.

E.5 Two-dimensional unsteady friction models

The nature of unsteady friction, as visualised using a boundary layer concept, is at least two-dimensional. In this regard, the use of two-dimensional models can both enhance the understanding of energy dissipation during a transient (including unsteady friction) and provide for the validation of one-dimensional models (such as one-dimensional acceleration based models).

The governing hyperbolic-parabolic partial differential equations for two-dimensional transient flow can be expressed using equations analogous to their one-dimensional counterparts for the conservation of continuity and momentum:

$$\frac{g}{a^2}\frac{\partial H}{\partial t} + \frac{\partial u}{\partial x} + \frac{1}{r}\frac{\partial rv}{\partial r} = 0 \tag{E-33}$$

$$\frac{\partial u}{\partial t} + g\frac{\partial H}{\partial x} - \frac{1}{r\rho}\frac{\partial r\tau}{\partial r} = 0 \qquad \text{(E-34)}$$

where r is the radial distance from the pipe centreline, $u(x, r, t)$ is the local longitudinal velocity, $v(x, r, t)$ is the local radial velocity and:

$$\tau = \rho\nu\frac{\partial u}{\partial r} - \rho\overline{u'v'} \text{ is the wall shear stress} \qquad \text{(E-35)}$$

with u' and v' equal to the longitudinal and radial velocity turbulent perturbations, respectively

Vardy and Hwang (1991) developed a two-dimensional model by solving the hyperbolic and parabolic parts of the continuity and momentum equations using the Method of Characteristics (MOC) and a finite difference scheme, respectively. However, the disincentive to use the model developed by Vardy and Hwang (1991), or any other two-dimensional model, is impractical computational requirements. Nevertheless, such models are important for one-dimensional model calibration. Furthermore, as computational capacity continues to improve, and more efficient schemes are developed, the use of two-dimensional models may become more feasible.

E.6 Laboratory verification and potential field effects of unsteady friction

The effects of unsteady friction have been noted in experimental investigations since Daily et al. (1956). More recently, Vitkovsky (2001) conducted a series of comprehensive laboratory investigations confirming the effect of unsteady friction for laminar flow in the experimental apparatus located at the University of Adelaide, South Australia (as described in Chapter 3). Vitkovsky (2001) experimentally confirmed the validity of a number of one-dimensional acceleration and weighting function models, including the model developed by Zielke (1968), using this apparatus.

However, despite the extensive theoretical development of unsteady friction models, and laboratory confirmation of the effect, most transient practitioners still either view the phenomena itself, or its effect, with scepticism. At the 9th International Conference on Pressure Surges in 2004 at Chester, UK, Alan Vardy, under questioning from United Kingdom operators, conceded that the effect of unsteady friction would vary for pipelines with different diameters, roughness and operational conditions (i.e., flows). However, he pointed out that the significance of the effect in the field could not be assessed until field tests were undertaken. Unfortunately, at the time of the conference, no such field test results were available and this lack of information clouded the debate. Controlled field tests on a large transmission pipeline, demonstrating the significance of unsteady friction in the field, at least for relatively low Reynolds number flows, are presented in this thesis.

Appendix F

Development of a solenoid valve operated transient generator

The use of solenoid valves to perform the rapid closure of a side discharge has been explored in the laboratories at the University of Adelaide. The use of solenoid valves in the field was complicated by the requirement for larger discharges at higher pressures. Numerous direct action solenoid valves were investigated. These valves comprise a direct plunger that is motivated by a solenoid coil mounted around the plunger's axis. The advantage in using these valves is that a response time (i.e., closure time) in the order of 5 to 10ms could be achieved. Unfortunately, neither "off the shelf" nor custom-made direct action solenoid valves were capable of closing across differential pressures of more than typically 25 to 50kPa with orifice sizes of 5 to 10mm.

As a consequence, the use of pilot operated solenoid valves was investigated. A diaphragm exists within the body of these valves which, when depressed, prevents flow through the valve body and discharge orifice. The position of this diaphragm is forced closed with a spring. However, this spring is finely balanced and will only remain closed when a back pressure pilot to the discharge side of the valve remains closed. A solenoid plunger controls the status of this pilot relief. For normally closed valves, the solenoid plunger is depressed when un-excited and prevents the relief of back pressure from behind the main diaphragm (and thus the valve remains closed). When the plunger is lifted (i.e., when it is excited), back pressure from behind the main diaphragm is relieved and the valve opens. A normally open valve can be configured by reversing the plunger position in its no excitation and excited positions.

A problem with pilot operated solenoid valves is the distortion of the flow through the valve and associated hydraulic losses. Furthermore, they have relatively slow response times. The fastest response time for an "off the shelf" pilot operated solenoid valve with normally open operation was 40ms. Two Asco Joucomatic pilot operated solenoid valves, SC E238A007 (12mm discharge orifice) and SC E238A009 (20mm discharge orifice), were purchased and installed on a standpipe for the generation of

side discharges in the field. Figure F-1 shows the installation of the SC E238A007 valve on a standpipe with side discharge after connection to the Saint Johns Terrace Pipeline (SJTP) in July 2002. Unfortunately, the technical specifications for the valves were not conservative and the fastest closing time that could be achieved was 60ms.

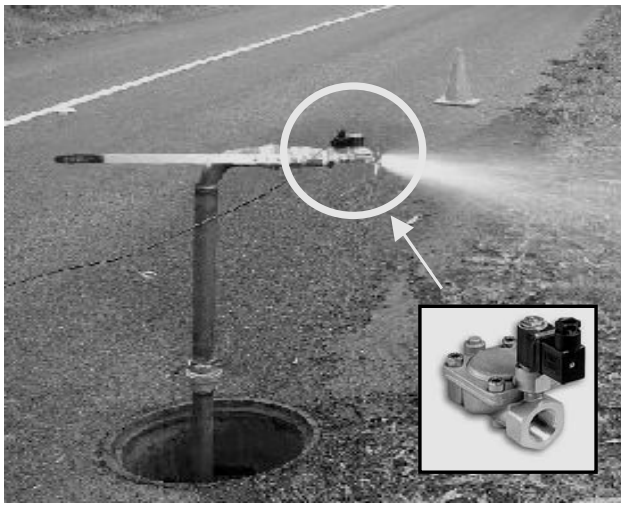

Figure F-1 – Pilot operated solenoid valve version of transient generator

Appendix G

Calibration of field pressure transducers

The field test dates mentioned in the thesis are summarised in Table G-1. It was necessary to calibrate each pressure transducer/amplifier combination, with associated data acquisition system, on dates that were as close as possible prior to and following the test dates. Table G-2 summarises the dates on which the pressure transducers were calibrated. A hand held pressure pump was used to pressurise the pressure transducers to predetermined levels (this hand held pressure pump was, in turn, checked using a dead weight calibration machine). The non-flush pressure transducer was not calibrated on the 9th and 16th July 2003 because it had not arrived from the UK.

Table G-1 – Summary of test dates on field pipeline and network systems

Field System	Test dates
HTP	20th and 21st May 2004
MTP	19th and 20th May and 11th and 12th August 2004
SJTP	23rd July, 15th August and 26th August 2003
KCP	28th August 2003
FSP	16th July and 7th August 2003
Willunga Network	2nd July, 31st July and 19th September 2003

Table G-2 – Calibration dates for pressure transducer/amplifier combinations

Calibration date	Flush face T1	Flush Face T2	Non-Flush T3
9/07/2003	Yes	Yes	No
16/07/2003	Yes	Yes	No
23/07/2003	Yes	Yes	Yes
29/07/2003	Yes	Yes	Yes
1/08/2003	Yes	Yes	Yes
25/08/2003	Yes	Yes	Yes
22/09/2003	Yes	Yes	Yes
18/05/2004	Yes	Yes	Yes
2/06/2004	Yes	Yes	Yes

Appendix G – Calibration of field pressure transducers

Figures G-1 and G-2 show the average voltage output from the pressure transducer/amplifier combinations for the two flush face Druck PDCR-810 transducers (taken over all the calibration results). The average relationship between output voltage and pressure is linear and the intercept remains at zero volts for zero pressure over the period between the 9th July 2003 and 2nd June 2004. Figures G-1 and G-2 also show the maximum variation from the average for all calibrations. The maximum and minimum envelopes confirm that there is no significant variation from the average for any of the calibrations.

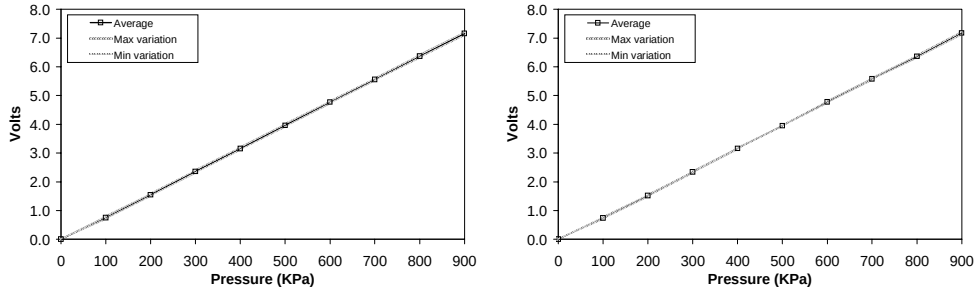

Figures G-1 and G-2 – Average relationship between output voltage and pressure for the flush face transducer/amplifier combinations T1 and T2, respectively

Figure G-3 shows the average voltage output from the pressure transducer/amplifier combinations for the non-flush face Druck PDCR-810 transducer (taken over all the calibration results). The average relationship between output voltage and pressure is again linear and the intercept remains at zero volts for zero pressure over the period between the 23rd July 2003 and 2nd June 2004. The maximum and minimum envelopes confirm that there is no significant variation from the average for any of the calibrations. The same flush face and non-flush face pressure transducer/amplifier combinations were used throughout the test period in order to avoid any variability associated with combining different pressure transducers and amplifiers.

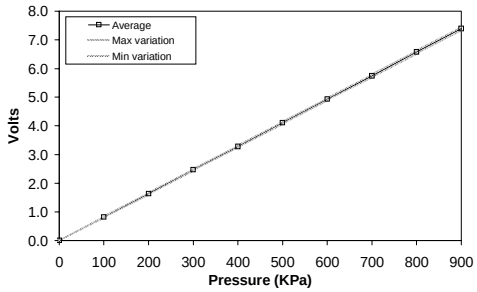

Figure G-3 – Average relationship between output voltage and pressure for the non-flush face transducer/amplifier combination

Appendix H

Transient generator nozzle calibration and laboratory apparatus

The calibration of the lumped discharge coefficients for the nozzles used in the transient generator was performed in the laboratories of the University of Adelaide by mounting the transient generator, complete with nozzle, in a pipeline system supplied by a roof tank located 4 floors above. The outflow from the roof tank supplies a 300mm diameter pipeline from the roof level down to the laboratories where a 100mm diameter horizontal offtake provides for the connection of the transient generator. The discharge from different nozzles is directed to a volumetric tank below where the measurement of depth over time allows the flow rate to be calculated. The volumetric tank is emptied into a sub-floor reservoir and pumped back to the roof tank using a fixed flow pump.

Table H-1 shows the calibrated discharge coefficients for the nozzles used in the transient generator. The discharge coefficients are calculated using the orifice equation and the measured discharges with a constant pressure head of 11.8m from the water level in the roof tank. The discharge coefficients have a constant value of 0.9 for nozzle sizes up to 10mm because the same smooth bore fitting was used. However, a lower discharge coefficient of 0.75 is obtained for the 15mm nozzle because a rough threaded fitting was used.

Table H-1 – Calibrated transient generator nozzle discharge coefficients

Nozzle Size (mm)	Area Nozzle (m^2)	Volumetric Tank Time (s)				Volume (m^3)	Discharge (m^3/s)	C_dA_L (x e 03)	C_d
		1	2	3	Avg.				
6	0.00002827	572.3	577.0	575.7	575.0	0.2185	0.000380	0.02498	0.9
7	0.00003848	424.2	423.9	427.4	425.2	0.2185	0.000514	0.03378	0.9
8	0.00005027	322.2	320.6	322.2	321.7	0.2185	0.000679	0.04465	0.9
9	0.00006362	509.8	509.7	510.4	510.0	0.4370	0.000857	0.05633	0.9
10	0.00007854	410.0	411.4	412.4	411.3	0.4370	0.001063	0.06985	0.9
15	0.00017671	213.6	214.3	213.5	213.8	0.4370	0.002044	0.13437	0.75*

* the discharge coefficient for the 15mm nozzle is lower because it was threaded

Figure H-1 below illustrates the arrangement in the laboratory used for the calibration of the different side discharge nozzles and a 100mm diameter field gate valve previously retrieved from the Willunga Network. The weir box and sharp crested weir were not used for flow measurement because of uncertainty regarding the calibrated discharge versus depth relationship (which could only be resolved by calibrating using the volumetric tank below).

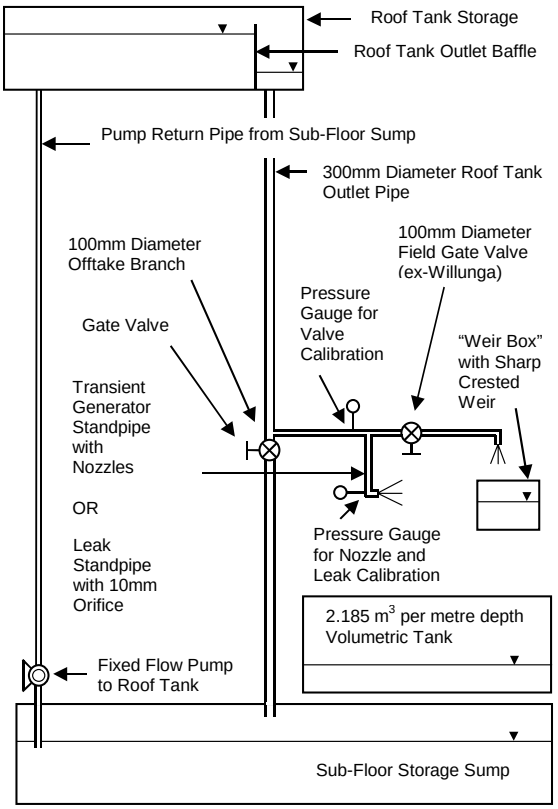

Figure H-1 – Laboratory configuration for transient generator nozzle and in-line gate valve calibration

Appendix I

Calibration of 100mm diameter in-line gate valve

I.1 Calibration of valve in the laboratory

An in-line gate valve (wedge type) was retrieved from United Water's depot as shown in Figure I-1. A typical cross-section and key dimensions identified by Idel'Chik (1960) are also shown. The valve was incrementally opened, from a closed position, to the positions specified in Table I-1 (below). Each valve position was examined, before the discharge pipeline was connected, to correlate the motion of the wedge gate with the number of turns of the valve spindle. The height of the opening between the wedge gate and seat increased proportionately with the thread and pitch of the spindle.

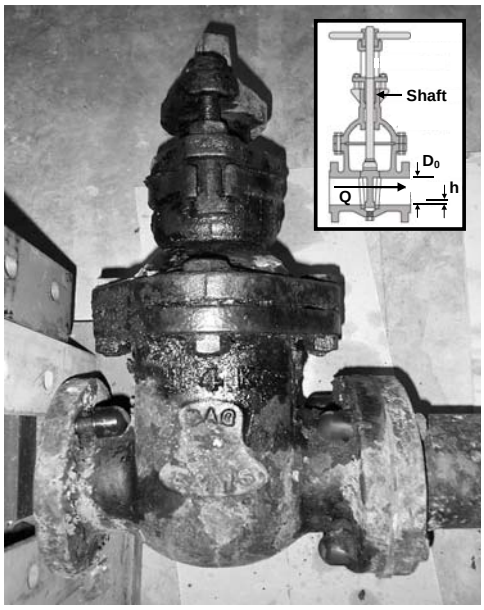

Figure I-1 – In-line gate valve (wedge type) retrieved from United Water's depot with cross-section view of typical gate valve (Idel'Chik (1960))

The pressure head immediately upstream of the valve was measured using a manual pressure gauge installed in a direct tapping. This pressure was confirmed using a pressure transducer in a second tapping and logging instrumentation. The pressure

head downstream of the valve was close to atmospheric as the downstream outlet pipe discharged horizontally to a nearby (less than 2m away) open "weir box" and then sub-floor volumetric tank below. The discharge through the valve at each incremental opening was measured using the sub-floor volumetric tank. A depth versus volume relationship of 2.185m^3 per metre of depth in the volumetric tank was used to calculate discharge. Table I-1 shows the time for the volume in the volumetric tank to increase in depth by 0.5m (i.e., the time for 1.093m^3 to accumulate in the tank).

Table I-1 – Laboratory measured discharge for various in-line gate valve openings using volumetric tank

Position No.	Valve Position	Volumetric Tank Time (s)				Flow from Tank (L/s)	Pressure Head (m)
		1	2	3	Avg.		
1	¼ turn	1292.7	1236.1	1217.2	1248.7	0.88	10.67
2	½ turn	451.2	435.6	432.5	439.8	2.48	10.54
3	¾ turn	234.7	237.6	234.7	235.7	4.64	10.28
4	1 turn	165.8	167.6	166.5	166.6	6.56	10.05
5	1¼ turns	125.7	125.5	128.6	126.6	8.63	9.88
6	1½ turns	103.4	103.8	103.8	103.7	10.54	9.40
7	1¾ turns	87.6	89.3	88.4	88.4	12.35	8.50
8	2 turns	76.4	78.3	77.7	77.5	14.11	7.89
9	2½ turns	62.0	62.2	63.3	62.5	17.48	6.90
10	3 turns	53.0	54.2	54.5	53.9	20.27	5.58
11	3½ turns	48.6	49.8	49.9	49.4	22.10	4.37
12	4 turns	45.6	47.2	47.1	46.6	23.43	3.28

Figure I-2 shows the relationship between the discharge and each incremental valve position determined using the volumetric tank. Figure I-3 shows the relationship between the measured pressure immediately upstream of the valve and the discharge for each incremental valve position. The pressure head decreases significantly for higher flows as the discharge through the valve approaches the capacity of the fixed speed pump returning water from the sump below the volumetric tank to the roof tank above. That said, for the range of valve positions presented (limited to a maximum of 4 turns open), a standing depth of water was maintained in the pipeline from the roof tank and the valve continued to control the flow through the system.

Appendix I – Calibration of 100mm diameter in-line gate valve

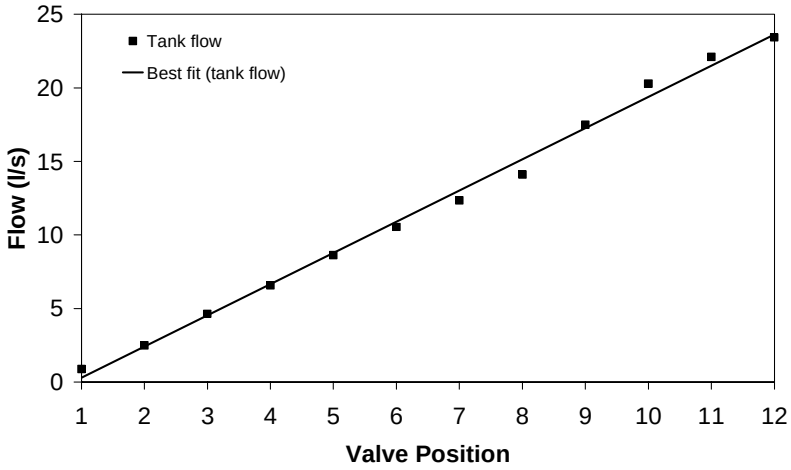

Figures I-2 – Calibrated flow versus valve position

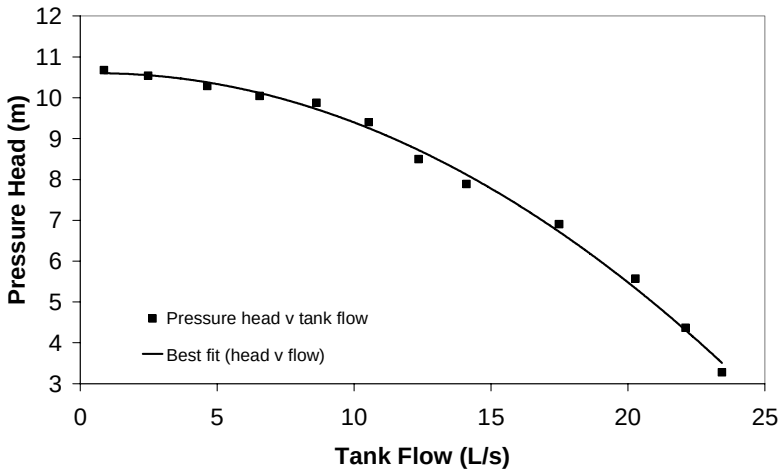

Figure I-3 – Calibrated pressure head versus flow

Knowing the discharge through the in-line gate valve and the pressure head immediately upstream, and that the downstream pressure is close to atmospheric, the following equation can be used to determine the loss factor (*K)* for each valve position:

$$K = \frac{2g\Delta H_V}{V^2} \qquad \text{(I-1)}$$

where ΔH_V is the differential pressure across the in-line valve and V is the velocity in the upstream 100mm nominal diameter pipe

Table I-2 summarises the calibrated loss factors corresponding to each incremental position and compares the results, where possible, with those experimentally determined by Idel'Chik (1960) for a similar in-line gate valve. The loss factors are of the same order of magnitude when the valve is between 2½ to 4 turns open (the only corresponding valve opening positions available from Idel'Chik (1960)).

Table I-2 – Calibrated loss factors for 100mm diameter in-line gate valve retrieved from the Willunga Network

Position No.	Valve Position	Opening h/Do*	Flow from Tank (L/s)	Head Loss (m)	K loss factor	K factor from Idel'Chik (1960)
1	¼ turn	0.025	0.875	10.67	16867.4	NA
2	½ turn	0.05	2.484	10.54	2065.5	NA
3	¾ turn	0.075	4.636	10.28	578.8	NA
4	1 turn	0.1	6.558	10.05	282.6	NA
5	1¼ turns	0.125	8.628	9.88	160.5	NA
6	1½ turns	0.15	10.539	9.40	102.4	NA
7	1¾ turns	0.175	12.352	8.50	67.4	NA
8	2 turns	0.2	14.108	7.89	47.9	NA
9	2½ turns	0.25	17.484	6.90	27.3	30
10	3 turns	0.3	20.273	5.58	16.4	22
11	3½ turns	0.35	22.102	4.37	10.8	17
12	4 turns	0.4	23.431	3.28	7.2	12

*where h (the height of the valve gate opening) and D_0 (the diameter of the pipeline) have been previously defined

Figure I-4 shows the relationship between the loss factors and incremental valve position. The in-line orifice equation is used in thesis to model the presence of discrete blockages. Hence, the equivalent orifices and discharge coefficients have been determined, for each incremental valve position and loss factor, as described below.

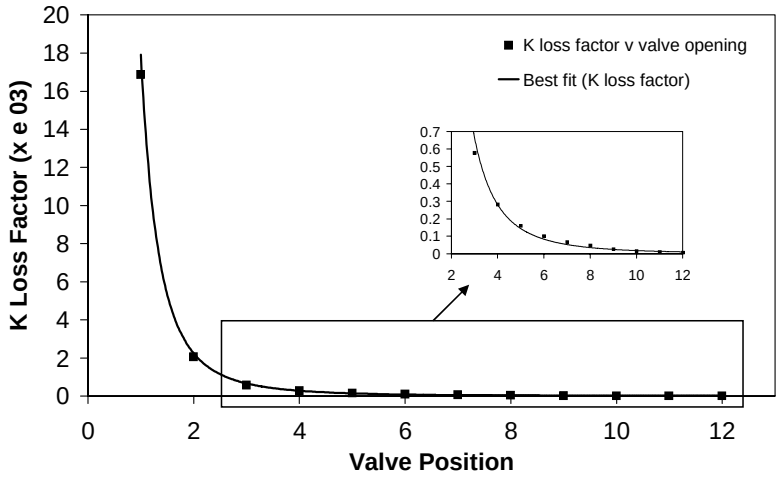

Figure I-4 – Loss factors calibrated in the laboratory for 100mm diameter in-line gate valve retrieved from the Willunga Network

I.2 Form of in-line valve equation

The loss factors determined above can be re-expressed, for each incremental valve position, in terms of equivalent orifices with discharge coefficients. This is done using the following equations:

$$V = \sqrt{\frac{2g\Delta H}{K}} \text{ and } Q_{valve} = A_P \sqrt{\frac{2g\Delta H}{K}} \quad \text{(I-2)}$$

where A_P is the area of the pipe upstream of the valve, ΔH is the pressure loss across the valve and K is the loss factor

Furthermore, the discharge through an equivalent in-line orifice can be determined using:

$$Q_{orf} = C_d A_V \sqrt{2g\Delta H} \quad \text{(I-3)}$$

where C_d is the discharge coefficient for the valve opening (or orifice) and A_V is the area of the valve opening (or orifice)

Combining equations I-2 and I-3 gives a relationship for the lumped orifice parameter in terms of the area of the pipe upstream of the valve and the loss factor (*K*):

$$C_d A_V = \sqrt{\frac{A_P^2}{K}} \tag{I-4}$$

Equation I-4 has been used to determine equivalent $C_d A_V$ values and orifice diameters for each incremental valve position as shown in Table I-3. While there is uncertainty regarding an appropriate C_d value for the opening between the valve wedge and seat, this is not critical provided the lumped orifice parameter is used in forward modeling and subsequent inverse analysis. That said, if C_d is given a value of 0.6, which is slightly lower than the typical value of 0.65, then the resultant values of A_V match geometric estimates of the opening area between the valve wedge and seat relatively accurately.

Table I-3 – Equivalent $C_d A_V$ values and diameters for various valve loss factors (*K*)

Position No.	Valve Position	Opening h/Do*	Pipe Area (m^2)	K loss factor	C_dA_V (x e 03)	C_d	A_V (x e 03)	Equivalent Diameter (mm)
1	¼ turn	0.025	0.00785	16867.4	0.0604	0.6	0.1007	11.3
2	½ turn	0.05	0.00785	2065.5	0.1727	0.6	0.2879	19.1
3	¾ turn	0.075	0.00785	578.8	0.3263	0.6	0.5438	26.3
4	1 turn	0.1	0.00785	282.6	0.4670	0.6	0.7783	31.5
5	1¼ turns	0.125	0.00785	160.5	0.6196	0.6	1.0327	36.3
6	1½ turns	0.15	0.00785	102.4	0.7757	0.6	1.2929	40.6
7	1¾ turns	0.175	0.00785	67.4	0.9562	0.6	1.5936	45.0
8	2 turns	0.2	0.00785	47.9	1.1342	0.6	1.8904	49.1
9	2½ turns	0.25	0.00785	27.3	1.5024	0.6	2.5040	56.5
10	3 turns	0.3	0.00785	16.4	1.9384	0.6	3.2307	64.1
11	3½ turns	0.35	0.00785	10.8	2.3887	0.6	3.9811	71.2
12	4 turns	0.4	0.00785	7.2	2.9255	0.6	4.8759	78.8

* where h (the height of the valve gate opening) and D_0 (the diameter of the pipeline) have been previously defined

Appendix J

Flowmeter data for the Hanson Transmission Pipeline and SCADA telemetry for the Willunga Network

J.1 Flowmeter data for the Hanson Transmission Pipeline

An insertion flowmeter was located along the Hanson Transmission Pipeline (HTP) (upstream of the Burra township pump station offtake). This flowmeter operates to continually monitor the flow in the HTP at a recording rate of 0.1Hz. An additional flowmeter was installed on the Burra township pump station offtake to continually monitor the flow pumped to the Burra township storage. The data from both insertion flowmeters is physically plotted on charts. These charts are removed each week and stored for record keeping purposes. The chart records for the week encompassing the test dates on the 20th and 21st May 2004, and showing the flow in the HTP and the Burra township pump station offtake, are reproduced in Figures J-1 and J-2. The Burra township pump station was inactive during the period of the transient tests.

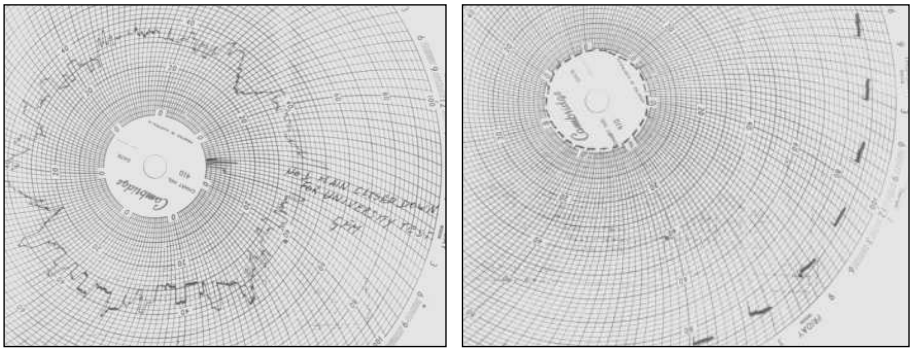

Figures J-1 and J-2 – Chart records for the Hanson Transmission Pipeline and Burra township pump station for the week encompassing the 20th and 21st May 2004

Figure J-3 focusses on the section of the chart for the HTP that shows the pipeline being shut down and then small flows being established for each transient test (either with or without a 9L/s). The chart record indicates that the flow in the HTP twice reached 9.5% of its maximum flow, and then twice reached 11.5% of its maximum

flow, in the period between 11am and 5pm on the 21st May 2004. These records corresponding to two transient tests conducted without a leak and two tests conducted with a 9L/s leak.

The maximum rated flow for the recorder is 450L/s and so the percentages correspond with flows of approximately 43L/s and 52L/s for the transient tests with and without a leak, respectively. The remainder of the records from the flowmeter confirm that the flow in the HTP was reduced to approximately 0L/s during the period between 11am and 5pm on the 21st May 2004. Figure J-4 shows a picture of the insertion flowmeter installation for the HTP.

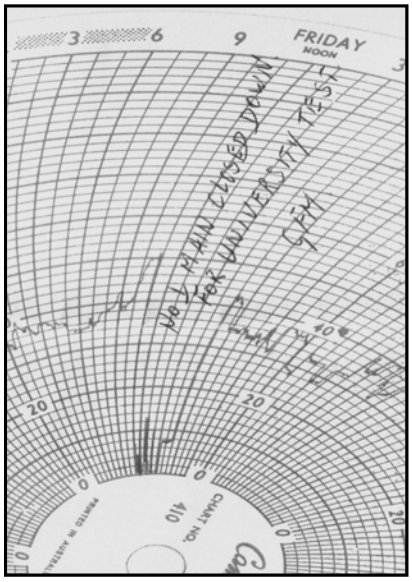

Figures J-3 and J-4 – Detailed view of HTP chart record during the period of the tests conducted on the 21st May 2004 and a picture of the insertion flowmeter

J.2 SCADA telemetry for the Willunga Network

The Willunga Network is supplied from a single tank that has water level telemetry recorded at 0.5hr intervals. Furthermore, the digital display from the tank depth gauge can be read within the Willunga pump station building at any time. Tank depth levels of 48.9% and 47.8% (giving a 1.1% reduction in depth over the intervening time period) were read from the digital display in the pump station building, at midnight

and 5.00am on the 31st July 2003, respectively. These values were more accurate than those later obtained from the SCADA history, recorded at 0.5hr intervals, but both sets of information were in general agreement. The SCADA history of the tank depth for a period of 14 days encompassing the night of the tests performed on the 31st July 2003 is shown in Figure J-5.

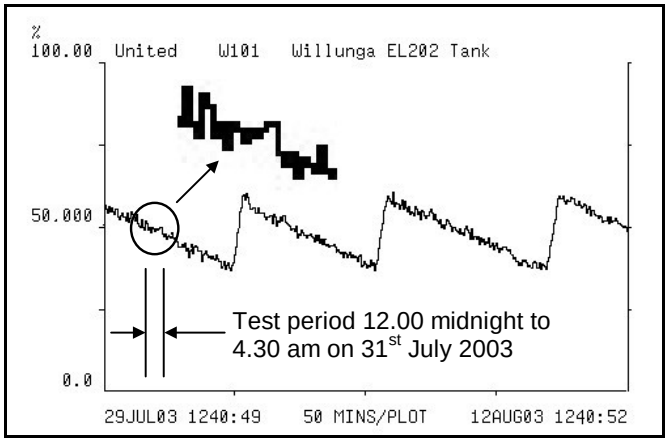

Figure J-5 – SCADA history of tank depth levels during testing period

Figure J-5 shows that the Willunga tank exchanges water over approximately a 4 day period in mid-winter. The tank has a maximum volume of 2.227ML and a depth to the outlet pipe obvert of 4.15m below the high water mark (relative level 202.2m). This information was used to determine that the 1.1% change in depth equated to a fall of 45.7mm in water level and that a volume of 22.4m^3 was drawn from the tank over the 5hr period between midnight and 5.00am on 31st July 2003.

Appendix K

Survey details of field transmission and distribution pipelines

K.1 Survey for transmission pipelines

The Hanson Transmission Pipeline (HTP)

The Hanson Transmission Pipeline (HTP) was surveyed using a global positioning survey (GPS) unit to accurately determine the relative position and elevation of the tank and downstream valve boundaries, lateral offtakes (both the Burra township pump station and Hanson township connections), in-line valve chambers, scour valves and air valves. Figures K-1 and K-2 show the alignment of the HTP in plan and elevation, respectively. This survey information was checked against information recorded on "as constructed" plans of the pipeline prepared shortly after it was first commissioned. The survey and "as constructed" information were in general agreement regarding the lengths and elevation of the HTP.

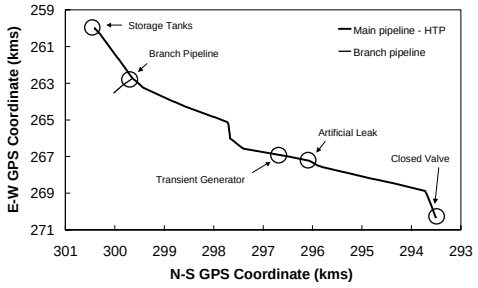

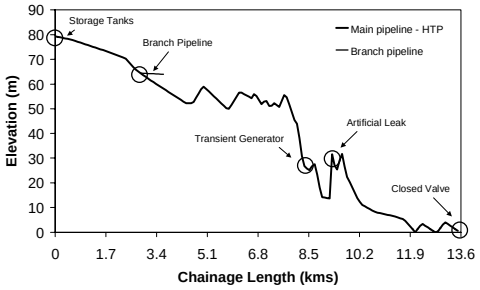

Figures K-1 and K-2 – GPS survey for the HTP in plan and elevation

The Morgan Transmission Pipeline (MTP)

The Morgan Transmission Pipeline (MTP) was surveyed using a global positioning survey (GPS) unit to accurately determine the relative position and elevation of the tank and valve boundaries, lateral offtakes (the Morgan township connection), in-line valve chambers, scour valves and air valves. Figures K-3 and K-4 show the alignment

of the MTP in plan and elevation, respectively. This survey information was checked against information recorded on "as constructed" plans of the pipeline prepared shortly after it was first commissioned. The survey and "as constructed" information were in general agreement regarding the lengths and elevation of the MTP.

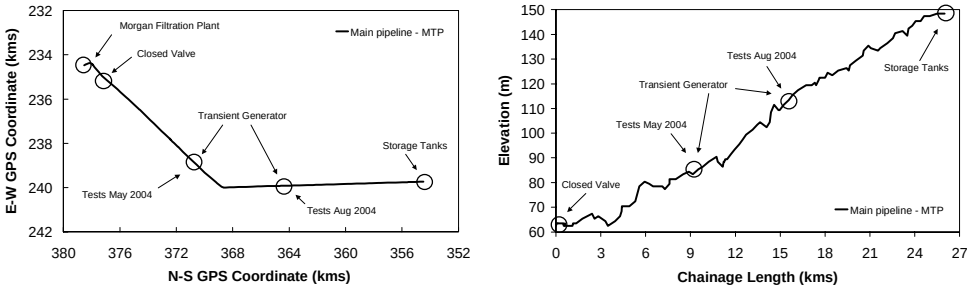

Figures K-3 and K-4 – GPS survey for the MTP in plan and elevation

K.2 Survey for distribution pipelines within the Willunga Network

The Saint Johns Terrace Pipeline (SJTP)

The Saint Johns Terrace Pipeline (SJTP) was manually surveyed, as part of a larger survey of the Willunga Network, using a "Total Station" electronic level and position survey instrument. Accurate elevation and position data was obtained for the "T" intersection, in-line gate valves, fire plugs and water service connections along the SJTP. Each in-line gate valve and fire plug chamber was individually examined to determine the depth to valve spindles and this information enabled the elevation of the centerline of the SJTP to be calculated (using dimensions measured from an equivalent in-line gate valve and fire plug).

Figures K-5 and K-6 show the alignment of the SJTP in plan and its profile in elevation, respectively. The water service network configurations shown at each service connection are idealised and not necessarily representative of the actual plumbing to various fixtures within each private residence. Survey information regarding the position and elevation of the SJTP was rigorously checked against information recorded in "as constructed" plans of the pipeline prepared immediately

after it was laid. The survey and "as constructed" information, regarding the lengths and elevations of the pipework comprising the SJTP, were consistent.

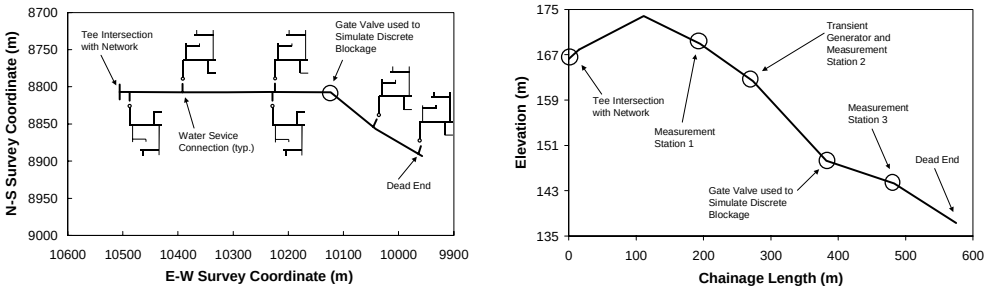

Figures K-5 and K-6 – Survey information for the SJTP in plan and elevation

The Kookaburra Court Pipeline (KCP)

The Kookaburra Court Pipeline (KCP) was manually surveyed, as part of a larger survey of the Willunga Network, using a "Total Station" electronic level and position survey instrument. Accurate elevation and position data was obtained for the "T" intersection, in-line gate valves, fire plugs and water service connections along the KCP. Each in-line gate valve and fire plug chamber was individually examined to determine the depth to valve spindles and this information enabled the elevation of the centerline of the KCP to be calculated (using dimensions measured from an equivalent in-line gate valve and fire plug).

Figures K-7 and K-8 show the alignment of the KCP in plan and its profile in elevation, respectively. The water service network configurations shown at each service connection are idealised and not necessarily representative of the actual plumbing to various fixtures within each private residence. Survey information regarding the position and elevation of the KCP was rigorously checked against information recorded in "as constructed" plans of the pipeline prepared immediately after it was laid. The survey and "as constructed" information, regarding the lengths and elevations of the pipework comprising the KCP, were consistent.

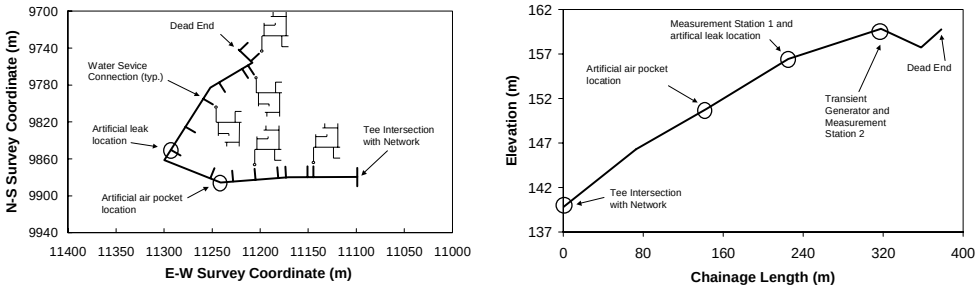

Figures K-7 and K-8 – Survey information for the KCP in plan and elevation

Appendix L

General transient test results for transmission pipelines

L.1 Summary of transient test results – Hanson pipeline

Results without the leak over a time period of 2L/a seconds

Figures L-1 and L-2 show the measured responses of the Hanson Transmission Pipeline (HTP), to controlled transient tests 1 and 2 (i.e., without a leak), over a period of 20s. The main features correspond to the initial pressure rise after the side discharge valve mounted in the transient generator is closed, a flat plateau until the reflection from the closed in-line valve at "Sheep Dip", a combination of superimposed reflections from the Burra township pump station offtake along the next plateau and, finally, the reflection from the Hanson Summit storage tanks. Both stations 1 and 2 record consistent features in the transient response.

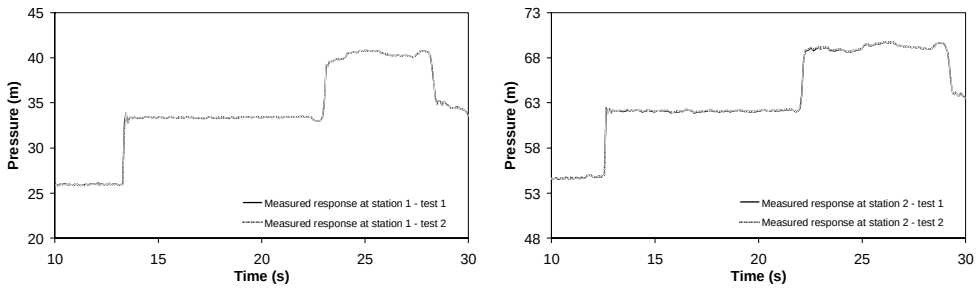

Figures L-1 and L-2 – Measured response of HTP without leakage for tests 1 and 2 over 20 seconds at stations 1 and 2, respectively

Results without the leak over a time period of 580 seconds

Figures L-3 and L-4 show the measured responses of the Hanson Transmission Pipeline (HTP), to controlled transient tests 1 and 2 (i.e., without a leak), over the duration of the measured response (i.e., 580s). Relative to the responses reported by Stoianov et al. (2003a) and Covas et al. (2004a), the measured responses are very

persistent and have an order of magnitude less damping. This may be attributed, to a degree, to the topological simplicity of the HTP and well-defined boundary conditions. That said, the measured responses from the HTP exhibit complexity related to the Burra township pump station offtake. Furthermore, it is apparent that the reflections from the closed in-line valve at "Sheep Dip", the Hanson Summit storage tanks and the Burra township pump station offtake all disperse rapidly leaving an amalgam waveform.

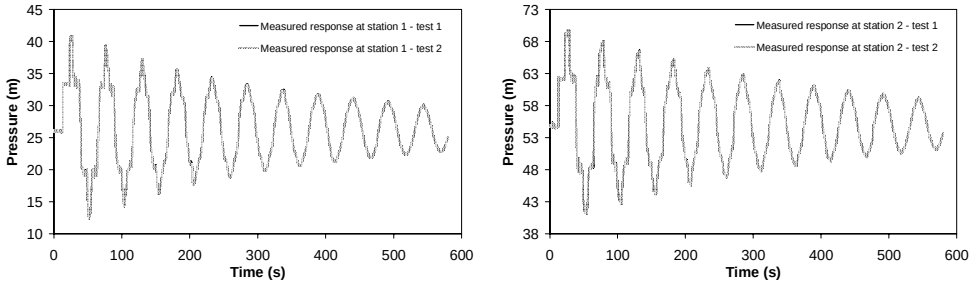

Figures L-3 and L-4 – Measured response of HTP without leakage for tests 1 and 2 over the duration of the measured response at stations 1 and 2, respectively

Results with the leak over a time period of 2L/a seconds

Figures L-5 and L-6 show the measured responses of the Hanson Transmission Pipeline (HTP), to controlled transient tests 3 and 4 (i.e., with a leak), over a period of 20s. As for the no-leak case, the main features correspond to the initial pressure rise after the side discharge valve mounted in the transient generator is closed, a flat plateau until the reflection from the closed in-line valve at "Sheep Dip", a combination of superimposed reflections from the Burra township pump station offtake along the next plateau and, finally, the reflection from the Hanson Summit storage tanks. Significantly, no reflection from the artificial 9L/s leak is discernable at this scale. A closer examination of the response is shown in the insets and reveals a weak leak reflection.

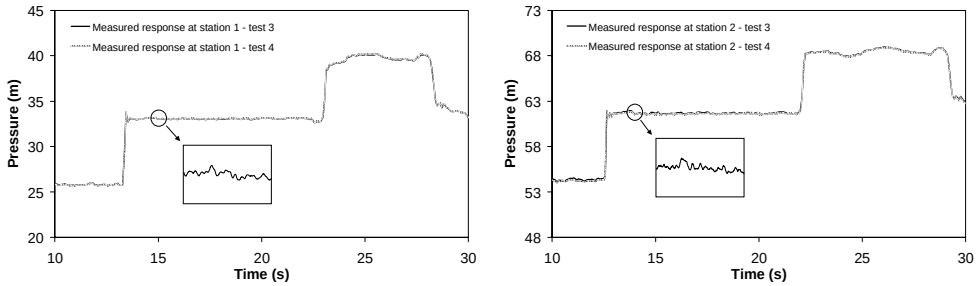

Figures L-5 and L-6 – Measured response of HTP with leakage for tests 3 and 4 over 20 seconds at stations 1 and 2, respectively

Results with the leak over a time period of 580 seconds

Figures L-7 and L-8 show the measured responses of the Hanson Transmission Pipeline (HTP), to controlled transient tests 3 and 4 (i.e., with a leak), over the duration of the measured response (i.e., 580s). It is apparent that the reflections from the closed in-line valve, the Hanson Summit storage tanks and the Burra township pump station offtake all disperse rapidly leaving an amalgam waveform. The damping effect of the leak is apparent even though only weak leak reflections are observed.

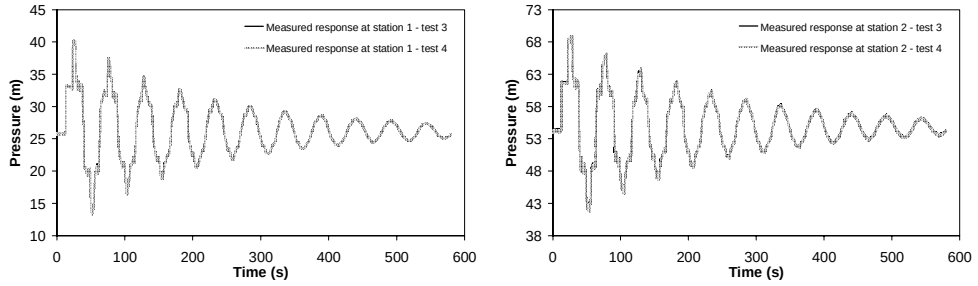

Figures L-7 and L-8 – Measured response of HTP with leakage for tests 3 and 4 over the duration of the measured response at stations 1 and 2, respectively

Comparison of results without and with a leak over 580 seconds

Figures L-9 and L-10 show the comparison between the measured responses of the Hanson Transmission Pipeline (HTP), to controlled transient tests 1 and 3, without

and with simulated leakage, respectively. As noted previously, it is apparent that the reflections from the closed in-line valve, the Hanson Summit storage tanks and the Burra township pump station offtake all disperse rapidly. Although not discernable at this scale, it is likely that the leak reflections in the response for test 3 are also dispersed. The cumulative damping effect of the leak is clearly discernable over the long term.

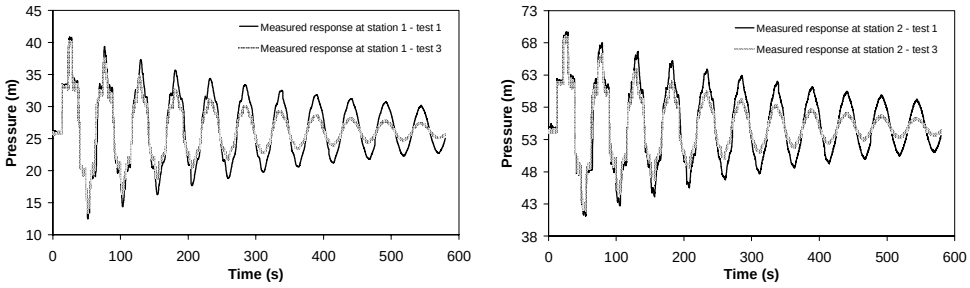

Figures L-9 and L-10 – Measured responses of the HTP without and with leakage, over the duration of the measured response, at stations 1 and 2, respectively

L.2 Summary of transient test results – Morgan pipeline

Results without an air pocket or blockage over a time period of L/a seconds

Figures L-11 and L-12 show the measured responses of the Morgan Transmission Pipeline (MTP), to controlled transient tests 1 and 2, conducted in May 2004, over a period of 20s, without any artificial air pocket or blockage. The main features correspond to the initial pressure rise after the side discharge valve mounted in the transient generator is closed, a flat plateau containing small reflections from two cross-connections and the reflection from the closed “No.1” in-line gate valve near the Morgan filtration/treatment plant. The reflections from the cross-connections are only apparent in the response measured at station 1 because of the close proximity of station 2 to the location of the cross-connections. The cross-connections comprise two 10m lengths of 700mm diameter pipeline before the in-line gate valves used to isolate the two parallel transmission pipelines are reached. In effect, two short stubs of 700mm diameter pipeline are attached to the MTP.

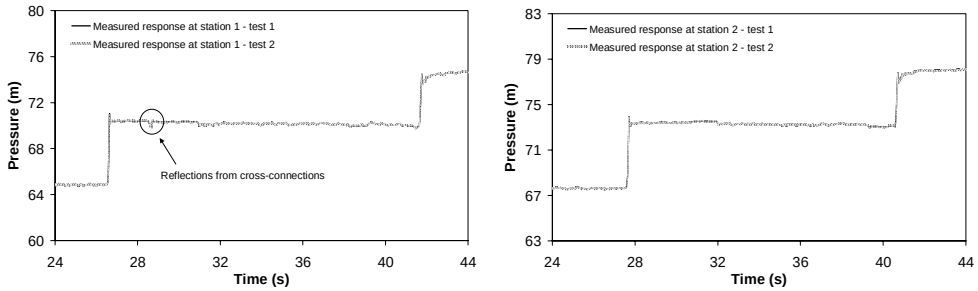

Figures L-11 and L-12 – Measured response of MTP for tests 1 and 2, conducted in May 2004, over 20 seconds at stations 1 and 2, respectively

Figures L-13 and L-14 show the measured responses of the MTP, to controlled transient tests 7, 8 and 9, conducted in August 2004, over a period of 10s, without any artificial air pocket or blockage. The difference between the tests is that the downstream boundary condition is formed by the closure of in-line gate valves "No.1", "No.2" and "No.3" for tests 7, 8 and 9, respectively. The response of the MTP over the first 10 seconds is very similar for all three tests and a consistent pattern of structured reflections is observed.

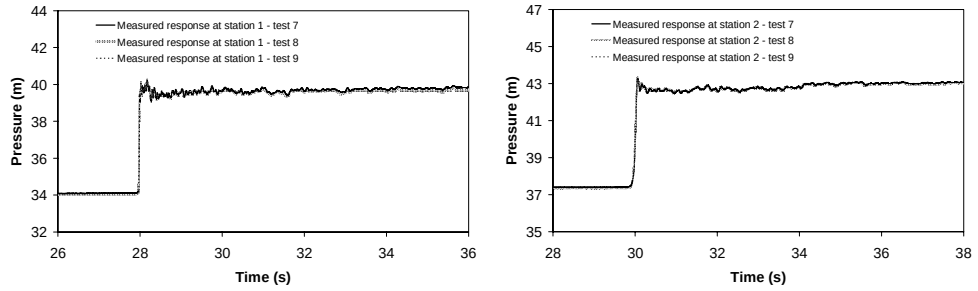

Figures L-13 and L-14 – Measured response of MTP for tests 7, 8 and 9, conducted in August 2004, over 10 seconds at stations 1 and 2, respectively

Figures L-15 and L-16 show the consistency in the response of the MTP to tests 7, 8 and 9. Despite different boundary conditions there is a repeated pattern of structured reflections. The reflections are sharper at station 1 than at station 2, which are 82m and 2478m from the location at which the controlled transient is induced,

respectively. That said, distinct reflection information is apparent at station 2. The observed reflections are considered in detail in this thesis and a potential application to the problem of internal wall condition assessment is presented.

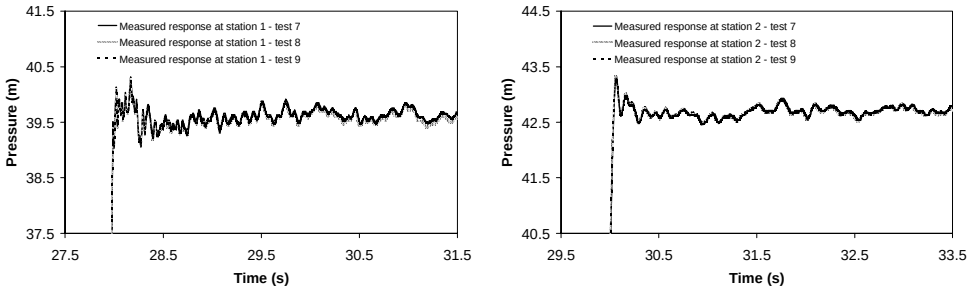

Figures L-15 and L-16 – Measured response of MTP for tests 7, 8 and 9, conducted in August 2004, over 4 seconds at stations 1 and 2, respectively

Results without an air pocket or blockage over a time period of 540 seconds

Figures L-17 and L-18 show the measured responses of the Morgan Transmission Pipeline (MTP), to controlled transient tests 1 and 2, conducted in May 2004, over the duration of the measured response (i.e., 540s), without any artificial air pocket or blockage. Again, relative to the responses reported by Stoianov et al. (2003a) and Covas et al. (2004a), the measured responses are more persistent and have less damping. That said, the reflections from the closed in-line gate valve "No.1" and the tanks disperse rapidly leaving an amalgam waveform.

An unexplained reflection corresponding to the position of in-line gate valve "No.5", at chainage 21546m, was noted. Closer examination of this reflection revealed that it took the form of a reflection expected from an air pocket. Furthermore, the pipeline had been recently opened and drained near the location of in-line gate valve "No.4" upstream of in-line gate valve "No.5". It was suspected that a small air pocket was trapped in close proximity to in-line gate valve "No.5".

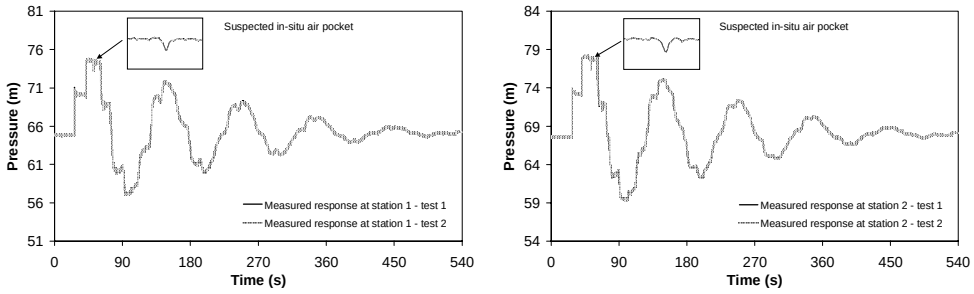

Figures L-17 and L-18 – Measured response of MTP for tests 1 and 2, conducted in May 2004, over duration of the measured response, at stations 1 and 2, respectively

Figures L-19 and L-20 show the measured responses of the MTP, to controlled transient tests 7, 8 and 9, conducted in August 2004, over the duration of the measured response (i.e., 540s), without any artificial air pocket or blockage. The significant differences between the response of the pipeline for test 7, conducted in August 2004, and tests 1 and 2, conducted in May 2004, are due to the change in the relative locations of the transient generator and measurement stations as described in the thesis. That said, the level of damping in the MTP, as configured with in-line gate valve "No.1" forming a downstream boundary condition, for tests 1 and 2, conducted in May 2004, and test 7, conducted in August 2004, is comparable.

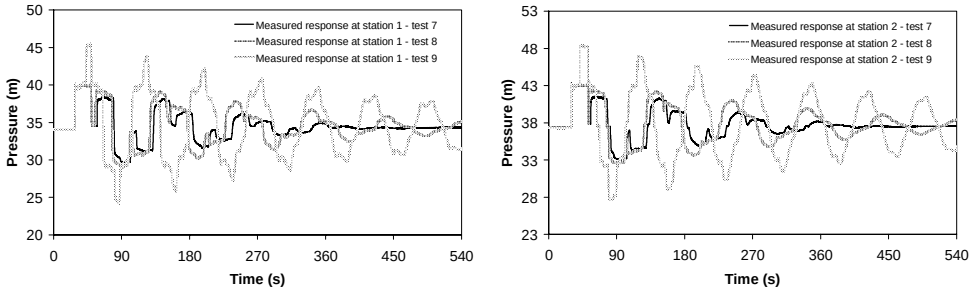

Figures L-19 and L-20 – Measured response of MTP for tests 7, 8 and 9, conducted in August 2004, over duration of the measured response, at stations 1 and 2, respectively

Figures L-19 and L-20 show that the level of damping for the MTP, configured with either in-line gate valve "No.1" or "No.2" closed to form the downstream boundary condition, is comparable for tests 7 and 8 (although the damping is marginally less for

test 8). In contrast, there is significantly less damping in the measured response of the MTP when configured with in-line gate valve “No.3” closed to form the downstream boundary condition. Potential reasons for this difference are explored in Chapter 7.

Results with an air pocket over a time period of L/a seconds

Figures L-21 and L-22 show the measured response of the Morgan Transmission Pipeline (MTP), to controlled transient test 3, conducted in May 2004, over a period of 20s, with an artificial 18.8L air pocket (compressed volume under 53m pressure). The measured response for test 1 is presented for comparison. The main features correspond to the initial pressure rise after the side discharge valve mounted in the transient generator is closed, a flat plateau containing distinct reflection from the artificially introduced air pocket, a smaller reflection from two cross-connections (apparent at station 1 only), a reflection from closed in-line valve “No.1” and, finally, a secondary reflection from the artificially introduced air pocket following the valve reflection.

Both stations 1 and 2 record consistent features in the transient response and the presence of the air pocket for test 3 is clearly discernable in comparison to test 1. The reflection from the artificially introduced air pocket takes a different form to that traditionally expected and in this regard is different from that from the suspected in-situ air pocket. The reason is the peculiar manner in which the artificial air pocket was introduced to the MTP (as described in Appendix T).

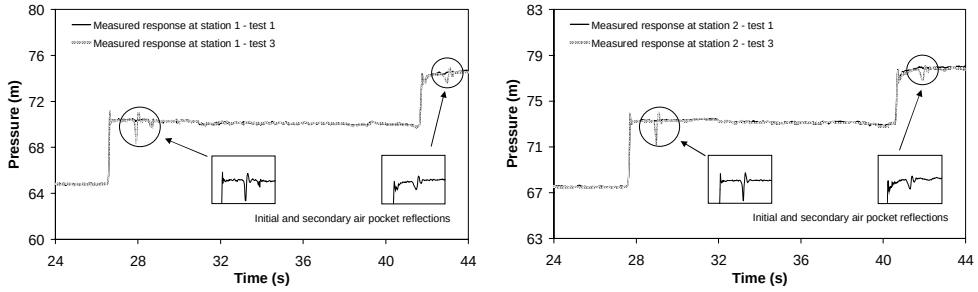

Figures L-21 and L-22 – Measured response of MTP, configured with an artificial air pocket for test 3, conducted in May 2004, over 20s, at stations 1 and 2, respectively

Despite the difference between the artificially introduced air pocket, and the likely configuration of an in-situ air pocket, the relative magnitude of the reflected responses should be similar. This is important as it means that tests 3 and 4, conducted in May 2004, can be used to gauge the size of the suspected in-situ air pocket (as previously noted). In this regard, the artificially introduced and in-situ air pockets appear to be of the same order of magnitude.

Results with an air pocket over a time period of 540 seconds

Figures L-23 and L-24 show the measured response of the Morgan Transmission Pipeline (MTP), to controlled transient test 3, conducted in May 2004, over the duration of the measured transient response (i.e., 540s), with an 18.8L artificial air pocket. The measured response for test 1 is presented for comparison. The presence of the air pocket gives rise to a barely perceptible increase in damping and the phase of the measured response is not discernibly different for tests 1 or 3. If the artificially introduced and in-situ air pockets are of the same order of magnitude, then the insensitivity of the measured response to test 3, with the artificial air pocket, in terms of damping and phase, suggests that the affect of the in-situ air pocket upon the measured response to test 1 (and 2) may also be relatively insignificant.

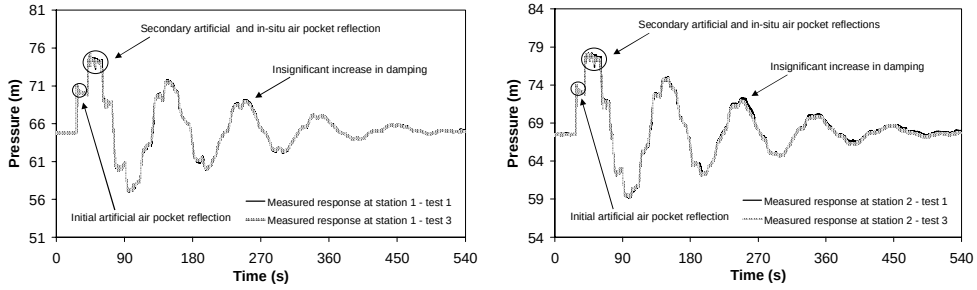

Figures L-23 and L-24 – Measured response of MTP, configured with an artificial air pocket for test 3, conducted in May 2004, over 540s, at stations 1 and 2, respectively

Results with a blockage over a time period of L/a seconds

Figures L-25 and L-26 show the measured response of the Morgan Transmission Pipeline (MTP), to controlled transient test 5, conducted in May 2004, over periods of 3.5 and 21s, for stations 1 and 2, respectively. The measured response for test 1 is presented for comparison. The 3.5s time scale is used to focus on the initial reflection from the partially closed in-line gate valve "No.3" and cross-connections at station 1. The 21s time scale is used to show the initial transmitted wavefront and reflection and subsequent secondary reflection, at station 2, from closed in-line gate valve "No.1" and partially closed in-line gate valve "No.3", respectively. As described in Chapter 6, in-line gate valve "No.3" was closed 54 of 58 turns to leave an equivalent open aperture of approximately 50mm equivalent diameter between the gate and seat of the valve.

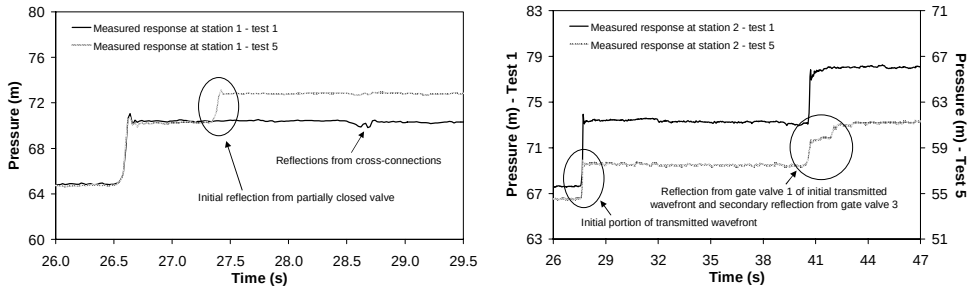

Figures L-25 and L-26 – Measured response of MTP, with an artificial blockage, for test 5, conducted in May 2004, over 3.5s and 21s time scales, respectively

Results with a blockage over a time period of 540 seconds

Figures L-27 and L-28 show the measured response of the Morgan Transmission Pipeline (MTP), to controlled transient test 5, conducted in May 2004, over the duration of the measured response (i.e., 540s), with an artificial blockage formed by the partial closure of in-line gate valve "No.3". The measured response for test 1 is presented for comparison. Significant differences are apparent over the first L/a and 2L/a seconds of the responses, associated with the reflections shown in Figures L-25

and L-26 above, as well as a change in the magnitude and form of the damped waveform.

The presented responses show the first field measurements of additional damping and secondary waveforms or frequencies associated with discrete blockages. The difficulty with using these measured responses to diagnose blockages generally in the field, as alluded to by Mohapatra et al. (2006), is likely to be other sources of damping and dispersion including, amongst other things, unsteady friction, entrained air, fluid structure interaction (FSI), mechanical motion and vibration, including flexural motion, and other forms of "viscous" damping caused by joints or soil/pipe interaction.

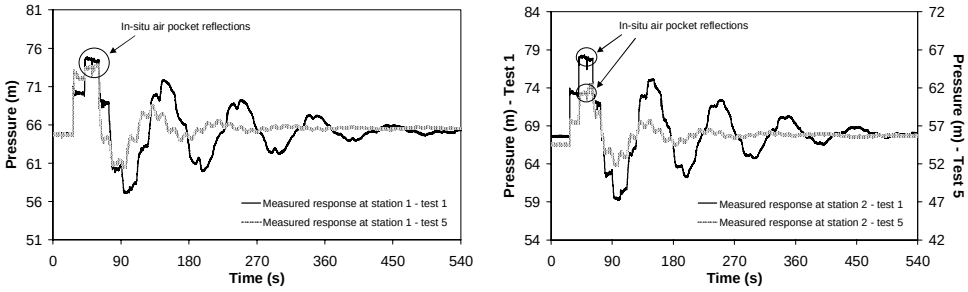

Figures L-27 and L-28 – Measured response of MTP, with an artificial blockage, for test 5, conducted in May 2004, over 540s, at stations 1 and 2, respectively